

**T.R.  
SAKARYA UNIVERSITY  
GRADUATE SCHOOL OF NATURAL AND APPLIED SCIENCES**

**STEADY-STATE MODEL OF A SINGLE-PHASE FULL-WAVE  
RECTIFIER WITH A CONSTANT VOLTAGE LOAD OPERATING  
IN DISCONTINUOUS MODE**

**MSc THESIS**

**Abdullah Waleed Jalil AL-SALIHI**

**Electrical and Electronics Engineering Department**

**FEBRUARY 2024**



**T.R.  
SAKARYA UNIVERSITY  
GRADUATE SCHOOL OF NATURAL AND APPLIED SCIENCES**

**STEADY-STATE MODEL OF A SINGLE-PHASE FULL-WAVE  
RECTIFIER WITH A CONSTANT VOLTAGE LOAD OPERATING  
IN DISCONTINUOUS MODE**

**MSc THESIS**

**Abdullah Waleed Jalil AL-SALIHI**

**Electrical and Electronics Engineering Department**

**Thesis Advisor: Assoc. Prof. Dr. Şuayb Çağrı YENER**

**FEBRUARY 2024**



The thesis work titled “**STEADY-STATE MODEL OF A SINGLE-PHASE FULL-WAVE RECTIFIER WITH A CONSTANT VOLTAGE LOAD OPERATING IN DISCONTINUOUS MODE**” prepared by Abdullah Waleed Jalil AL-SALIHI was accepted by the following jury on 08/02/2024 by unanimously/majority of votes as a MSc THESIS in Sakarya University Graduate School of Natural and Applied Sciences, Electrical and Electronics Engineering department.

### Thesis Jury

**Head of Jury :**      **Assoc. Prof. Dr. Şuayb Çağrı YENER** (Advisor)      .....  
Sakarya University

**Jury Member :**      **Prof. Dr. Aşkın DEMİRKOL**      .....  
Sakarya University

**Jury Member :**      **Assoc. Prof. Dr. Reşat MUTLU**      .....  
Tekirdağ Namık Kemal University



## **STATEMENT OF COMPLIANCE WITH THE ETHICAL PRINCIPLES AND RULES**

I declare that the thesis work titled "STEADY-STATE MODEL OF A SINGLE-PHASE FULL-WAVE RECTIFIER WITH A CONSTANT VOLTAGE LOAD OPERATING IN DISCONTINUOUS MODE", which I have prepared in accordance with Sakarya University Graduate School of Natural and Applied Sciences regulations and Higher Education Institutions Scientific Research and Publication Ethics Directive, belongs to me, is an original work, I have acted in accordance with the regulations and directives mentioned above at all stages of my study, I did not get the innovations and results contained in the thesis from anywhere else, I duly cited the references for the works I used in my thesis, I did not submit this thesis to another scientific committee for academic purposes and to obtain a title, in accordance with the articles 9/2 and 22/2 of the Sakarya University Graduate Education and Training Regulation published in the Official Gazette dated 20.04.2016, a report was received in accordance with the criteria determined by the graduate school using the plagiarism software program to which Sakarya University is a subscriber, I accept all kinds of legal responsibility that may arise in case of a situation contrary to this statement.

08/02/2024

Abdullah Waleed Jalil AL-SALIHI





*To my mother, father, and sisters.*



## **ACKNOWLEDGMENTS**

I would like, first, to thank Allah and praise Him for His generosity and care, which we experience daily. For all the good people who were supportive when I needed them, I would like to start by expressing my sincere gratitude to my advisor, Assoc. Prof. Dr. Şuayb Çağrı YENER, who spared no effort to help me through this study, and for his patience and guidance.

I would also like to dedicate special thanks to Assoc. Prof. Dr. Reşat MUTLU for sharing his valuable knowledge and experience with me. To all my friends who were a source of inspiration throughout the difficulties, thank you.

I want to express my deepest gratitude to my family—my dear mother, who never stopped being supportive in every possible way, my dear departed father, and my beloved sisters, thank you from the bottom of my heart.

Abdullah Waleed Jalil AL-SALIHI



## TABLE OF CONTENTS

	<u>Page</u>
<b>ACKNOWLEDGMENTS</b> .....	<b>ix</b>
<b>TABLE OF CONTENTS</b> .....	<b>xi</b>
<b>ABBREVIATIONS</b> .....	<b>xiii</b>
<b>SYMBOLS</b> .....	<b>xv</b>
<b>LIST OF FIGURES</b> .....	<b>xvii</b>
<b>SUMMARY</b> .....	<b>xxi</b>
<b>ÖZET</b> .....	<b>xxiii</b>
<b>1. INTRODUCTION</b> .....	<b>1</b>
1.1. Literature Review .....	1
1.2. Motivation of the Study.....	3
1.3. Content and Organization of the Thesis .....	3
<b>2. ANALYTICAL MODEL AND RECTIFIER SYSTEM</b> .....	<b>5</b>
2.1. Contextual Framework .....	5
2.2. A Brief Overview of Diodes .....	5
2.3. Rectifier Circuits .....	6
2.3.1. The full-wave bridge-rectifier circuit.....	7
2.3.2. Rectifier circuit with smoothing inductor and constant load .....	8
2.4. Conduction Modes of the Rectifier .....	9
2.5. Derivation of the Steady State Analytical Model.....	11
<b>3. SIMULATION OF THE RECTIFIER SYSTEM</b> .....	<b>19</b>
3.1. The Electrical Characteristics of the Rectifier System.....	19
3.2. Simulation Results of PSpice .....	19
3.2.1. Reducing the smoothing inductor's inductance .....	22
3.2.2. The continuous conduction mode .....	23
3.3. Simulation Results of Simulink.....	24
3.3.1. Reducing the smoothing inductor's inductance .....	26
3.3.2. The continuous conduction mode .....	27
3.4. The Relation Between the Conduction Angles .....	29
<b>4. THE EXPERIMENTAL RESULTS</b> .....	<b>33</b>
4.1. Elements of the Implemented Rectifier System .....	33
4.1.1. The autotransformer (variac) .....	33
4.1.2. The isolation transformer .....	35
4.1.3. The AC side smoothing inductor .....	36
4.1.4. The single-phase bridge rectifier.....	37
4.1.5. Lead-acid battery as a constant voltage load .....	38
4.2. The Measurement System .....	39
4.2.1. SCPI instrument control language .....	39
4.2.2. The oscilloscope.....	40
4.2.3. The current measurement probe.....	41
4.3. Acquiring the Experimental System's Electrical Measurements .....	43
4.3.1. Operating the experimental system.....	44
4.3.2. The autonomous measurement and data processing algorithm .....	45

4.3.3. Measurement results of the experimental system .....	47
4.3.4. A higher current measurement case .....	49
4.4. The Relation Between the Conduction Angles .....	51
4.5. Calculating the Time Constant of the Circuit.....	56
<b>5. CONCLUSION.....</b>	<b>57</b>
<b>REFERENCES .....</b>	<b>59</b>
<b>CURRICULUM VITAE .....</b>	<b>63</b>

## **ABBREVIATIONS**

<b>AC</b>	: Alternating Current
<b>ADC</b>	: Analogue to Digital Converter
<b>APE</b>	: Absolute Percentage Error
<b>CCM</b>	: Continuous Conditioning Mode
<b>DC</b>	: Direct Current
<b>DCM</b>	: Discontinuous Conditioning Mode
<b>RMS</b>	: Root Mean Square





## SYMBOLS

$V_s$	: Source Voltage
$V_m$	: Input Voltage Amplitude
$V_{dc}$	: DC Voltage
$V_F$	: Forward Voltage
$V_{out}$	: Output Voltage
$R$	: Resistance
$R_{battery}$	: Internal Resistance of the Battery
$r_s$	: Series Resistance of the Diode
$L$	: Inductance
$C$	: Capacitance
$X_L$	: Inductive Reactance
$i_s$	: Source Current
$i_{rec}$	: Rectifier Current
$\omega$	: Angular Frequency
$f$	: Frequency
$t$	: Time
$t_1$	: Time at Which the Conduction Occurs
$t_2$	: Time at Which the Conduction Stops
$T$	: Period of the Function
$\tau$	: Time Constant of the Circuit
$\alpha_1$	: Electrical Turn-On Angle
$\alpha_2$	: Electrical Turn-Off Angle
$n_1$	: Number of the Primary Winding Turns
$n_2$	: Number of the Secondary Winding Turns



## LIST OF FIGURES

	<u>Page</u>
<b>Figure 2.1.</b> (a) The P-N junction, (b) Practical diode appearance, and (c) Diode symbol. ....	6
<b>Figure 2.2.</b> The voltage-current characteristics of a Schottky diode. ....	6
<b>Figure 2.3.</b> (a) Bridge-rectifier with resistive load, (b) AC input voltage, (c) Rectified output voltage. ....	7
<b>Figure 2.4.</b> (a) Bridge-rectifier with capacitor filter and resistive load, (b) AC input voltage, (c) Rectified full-wave voltage, and (d) Capacitor-filtered DC output voltage. ....	8
<b>Figure 2.5.</b> The rectifier circuit with a current smoothing inductor at the input side, (a) Feeding a constant voltage load, and (b) Feeding a resistive load with a capacitor filter. ....	9
<b>Figure 2.6.</b> The AC source voltage and source current versus time for (a) The discontinuous conduction mode, and (b) The continuous conduction mode. ....	9
<b>Figure 2.7.</b> The rectifier circuit topology with an input smoothing inductor in case of (a) Feeding a battery load, and (b) Feeding an RC load. ....	10
<b>Figure 2.8.</b> The equivalent circuit when diodes are conducting in case of (a) Feeding a battery load, and (b) Feeding an RC load. ....	10
<b>Figure 2.9.</b> The equivalent circuit when diodes are not conducting with (a) A battery load, and (b) An RC load. ....	10
<b>Figure 2.10.</b> The numerical solution result and the curve fitting for $\alpha_1$ vs. $\alpha_2$ . ....	13
<b>Figure 2.11.</b> $\alpha_1$ vs. $\alpha_2$ for both the numerical result with the linear regression and approximated line. ....	16
<b>Figure 2.12.</b> The complementary relation between the conduction angles ( $\alpha_1$ and $\alpha_2$ ) and the input voltage amplitude. ....	16
<b>Figure 2.13.</b> The complementary relation of the plots of $\alpha_2$ vs. $V_{dc}/V_m$ and $\alpha_1$ vs. $V_{dc}/V_m$ . ....	17
<b>Figure 3.1.</b> The rectifier circuit schematic in OrCAD Capture. ....	20
<b>Figure 3.2.</b> Simulation result of PSpice for (a) Input voltage, and (b) Input current. ....	21
<b>Figure 3.3.</b> Simulation result of PSpice for (a) Output voltage, and (b) Output current. ....	21
<b>Figure 3.4.</b> Simulation results for (a) The input voltage, and (b) The input current when the smoothing inductor's inductance is reduced to 50 $\mu$ H. ....	22
<b>Figure 3.5.</b> Simulation results for (a) The output voltage, and (b) The output current when the smoothing inductor's inductance is reduced to 50 $\mu$ H. ....	22
<b>Figure 3.6.</b> (a) The input voltage, and (b) The input current, when $V_m = 25$ V. ....	23
<b>Figure 3.7.</b> (a) The output voltage, and (b) The output current, when $V_m = 25$ V. ....	23
<b>Figure 3.8.</b> (a) The input voltage, and (b) The input current, when $V_m = 40$ V. ....	24
<b>Figure 3.9.</b> (a) The output voltage, and (b) The output current, when $V_m = 40$ V. ....	24
<b>Figure 3.10.</b> Block diagram of the rectifier circuit drawn in Simulink. ....	25

<b>Figure 3.11.</b> Simulation result of Simulink for (a) Input voltage, and (b) Input current.....	26
<b>Figure 3.12.</b> Simulation result of Simulink for (a) Output voltage, and (b) Output current.....	26
<b>Figure 3.13.</b> Simulation results for (a) The input voltage, and (b) The input current when the smoothing inductor's inductance is adjusted to 50 $\mu\text{H}$ .....	27
<b>Figure 3.14.</b> Simulation results for (a) The output voltage, and (b) The output current when the smoothing inductor's inductance is adjusted to 50 $\mu\text{H}$ .....	27
<b>Figure 3.15.</b> Simulation result of (a) Input voltage, and (b) Input current when $V_m=25\text{V}$ .....	28
<b>Figure 3.16.</b> Simulation result of (a) Output voltage, and (b) Output current when $V_m=25\text{ V}$ .....	28
<b>Figure 3.17.</b> Simulation result of (a) Input voltage, and (b) Input current when $V_m=40\text{V}$ .....	29
<b>Figure 3.18.</b> Simulation result of (a) Output voltage, and (b) Output current when $V_m=40\text{ V}$ .....	29
<b>Figure 3.19.</b> $\alpha_1$ vs. $\alpha_2$ from simulation results and numerical results.....	31
<b>Figure 3.20.</b> The absolute percentage error of $\alpha_2$ values between the numerical result and the Simulink simulation result as a function of $\alpha_1$ .....	31
<b>Figure 3.21.</b> The absolute percentage error of $\alpha_2$ values between the numerical result and the PSpice simulation result as a function of $\alpha_1$ .....	32
<b>Figure 4.1.</b> Block diagram of the complete experimental system. ....	33
<b>Figure 4.2.</b> (a) The schematic of a standard step-down autotransformer, and (b) The construction of a typical autotransformer.....	34
<b>Figure 4.3.</b> The experimentally used autotransformer (variac). ....	35
<b>Figure 4.4.</b> The three inductor models that have been tested with the circuit. ....	37
<b>Figure 4.5.</b> The implemented rectifier circuit was made using MBR560 Schottky diodes.....	38
<b>Figure 4.6.</b> The lead acid batteries that have been used in the experiment. ....	38
<b>Figure 4.7.</b> The basic communication algorithm between the computer and the oscilloscope using SCPI commands.....	40
<b>Figure 4.8.</b> The oscilloscope model used for electrical measurements of the circuit. ....	41
<b>Figure 4.9.</b> The working principle of the Hall effect sensor. ....	42
<b>Figure 4.10.</b> The practically used current measurement probe. ....	43
<b>Figure 4.11.</b> The complete experimental system.....	44
<b>Figure 4.12.</b> The waveform data and signal properties acquiring algorithm. ....	46
<b>Figure 4.13.</b> Schematic of the implemented rectifier circuit with the measurement probes being connected. ....	47
<b>Figure 4.14.</b> The experimental circuit's measurements made with the 12 Ah battery load, for (a) Input voltage, and (b) Input current.....	48
<b>Figure 4.15.</b> The experimental circuit's measurements made with the 12 Ah battery load, for (a) Output voltage, and (b) Output current. ....	48
<b>Figure 4.16.</b> The experimental circuit's measurements made with the 9 Ah battery load, for (a) Input voltage, and (b) Input current.....	49
<b>Figure 4.17.</b> The experimental circuit's measurements made with the 9 Ah battery load, for (a) Output voltage, and (b) Output current. ....	49
<b>Figure 4.18.</b> Input voltage waveform for (a) The experimental rectifier circuit, and (b) PSpice.....	50

<b>Figure 4.19.</b> Input current waveform for (a) The experimental rectifier circuit, and (b) PSpice.....	50
<b>Figure 4.20.</b> Output voltage waveform for (a) The experimental rectifier circuit, and (b) PSpice. ....	51
<b>Figure 4.21.</b> Output current waveform for (a) The experimental rectifier circuit, and (b) PSpice. ....	51
<b>Figure 4.22.</b> The relation between $\alpha_1$ and $\alpha_2$ calculated from both the numerical solution and the experiment when the 12 Ah battery was used. ....	53
<b>Figure 4.23.</b> The relation between $\alpha_1$ and $\alpha_2$ calculated from both the numerical solution and the experiment when the 9 Ah battery was used. ....	53
<b>Figure 4.24.</b> The calculated results from the numerical solution, the approximated line, the simulation, and the experiment with the 12 Ah battery. ....	54
<b>Figure 4.25.</b> The calculated results from the numerical solution, the approximated line, the simulation, and the experiment with the 9 Ah battery. ....	54
<b>Figure 4.26.</b> The absolute percentage error of $\alpha_2$ values between the numerical and the experimental results as a function of $\alpha_1$ when using the 12 Ah battery. ....	55
<b>Figure 4.27.</b> The absolute percentage error of $\alpha_2$ values between the numerical and the experimental results as a function of $\alpha_1$ when the 9 Ah battery was used. ....	56



# **STEADY-STATE MODEL OF A SINGLE-PHASE FULL-WAVE RECTIFIER WITH A CONSTANT VOLTAGE LOAD OPERATING IN DISCONTINUOUS MODE**

## **SUMMARY**

Rectifiers are essential elements of the electrical circuits that require AC to DC voltage conversion, their operation can occur either in continuous conduction mode (CCM) or discontinuous conduction mode (DCM). When a rectifier operates in discontinuous current conduction mode, the current waveform will have conduction and zero-current intervals describable by current's turn on and turn off angles. This research's main aim is to analyse that behaviour.

An analytical model is developed for a single-phase full-wave bridge rectifier having an AC side smoothing inductor and a constant voltage load, operating in discontinuous conduction mode, after making the necessary assumptions for the simplified version of the model to be derived. The model derivation led to a nonlinear equation that describes the relation between the conduction angles of the input current, which was solved numerically using MATLAB, the numerical solution led to an almost linear relation between the conduction angles, which can also be represented by simply using the equation of line.

Simulations of the proposed rectifier circuit are carried out using PSpice and MATLAB's Simulink software to analyse the circuit operation and to find the correct parameter adjustments that need to be made to determine the circuit working mode and achieve the desired circuit characteristics, the relation between the conduction angles was also conducted from the simulation results and was plotted to show if it also satisfies the near-linear relation between the conduction angles, it was found that the maximum percentage error between the results gained from the theory compared to the simulation results was 14.4%.

The experimental circuit implementation was also done, the utility electricity with its near-sinusoidal voltage waveform was used to supply an autotransformer (variac) with electrical power, which was followed by a step-down isolation transformer, the output of that transformer fed the rest of the system, the reason behind using a variac was to have the ability to adjust the input voltage amplitude to any desired value for the required testing conditions, that will vary the amplitude of the electrical current flowing through the circuit, hence achieving a useful range of conduction angles.

Schottky diodes were used for the rectifier circuit, since they have low forward voltage rating. As this research requires a constant voltage load, 12 V, 12 Ah and 9 Ah, rated lead-acid, sealed batteries were used at the output of the rectifier circuit, and it was shown that a lead-acid battery was a good choice to be used as a constant load, and it fulfilled the need behind it in this research, and the rectifier system can also be used as an affordable battery charging system.

A Hall effect sensor-based current probe was used to carry out the current measurements. The acquired electrical measurement data was transferred to the

personal computer, then processed and plotted properly utilizing an autonomous measurement system, that shows the measurement readings on the computer easily and enables a code-based automated detection of the conduction angles.

The relation between the conduction angles acquired from the experimental system was presented and found that the results gained from the theoretical and experimental approaches showed support for each other, where the conduction angles kept having an almost linear relation between them across a wide range of test cases, by making use of maximum tolerable currents of the circuit components. The result of the maximum error calculation between the numerical solution and the experimental findings was 16.65% when the input voltage amplitude was 14.28 V for the 12 Ah battery.

The values of the turn off angles ( $\alpha_2$ ) obtained from the simulation and experiment were less than their values obtained from the numerical solution. It is believed that the effect of  $I \cdot R$  in the circuit behaves as if a reverse polarized voltage source whose value changes by the effect of the current is connected to the circuit, that's why the effective source voltage magnitude decreases, resulting in decreasing  $\alpha_2$  values.



## **SABİT YÜK GERİLİMİNE SAHİP SÜREKSİZ MODDA ÇALIŞAN TEK FAZLI TAM DALGA DOĞRULTUCUNUN KARARLI HAL MODELİ**

### **ÖZET**

Doğrultucular, güç dönüşümü gerektiren elektrik devrelerinin temel bileşenleridir. Doğrultma işlemi sürekli iletim modunda (CCM) veya süreksiz iletim modunda (DCM) gerçekleşebilir. Bir doğrultucu kesintili akım iletim modunda çalıştığında, akım karakteristiğinde sıfır-akım aralıkları ve buna karşılık akımın iletime girme ve çıkma açıları ortaya çıkar. Bu araştırmada bu davranışın analizine odaklanılmaktadır.

Bir fazlı tam dalga köprü doğrultucusunun basitleştirilmiş modelinin türetilmesi için temel varsayımlar yapıldıktan sonra, giriş hattında düzgülendirme indüktörü (şok bobini) olan ve sabit bir gerilim yüküne sahip yapının modeli ve analitik çözümü üzerine çalışılmıştır. Modelin türetilmesinde giriş akımının iletime girme ve çıkma (iletim) açıları arasındaki ilişkiyi tanımlayan bir doğrusal olmayan denklem ortaya çıkmaktadır. Doğrusal olmayan bu denklemin analitik olarak çözülmesi mümkün olmadığı için MATLAB programı kullanılarak numerik çözümü yapılmıştır. Numerik çözüm ile iletim açıları arasında çok yaklaşık olarak doğrusal bir ilişki elde edilmiş olup, iletim açıları arasındaki ilişki eğri uydurma metodu kullanılarak tanımlanmıştır. Ayrıca, iletim açıları, giriş geriliminin genliğine göre çizildiğinde aralarındaki tamamlayıcı bir ilişki olduğu görülmektedir ve giriş gerilim genliği azaltıldığında iletim açılarının  $90^\circ$ 'de kesişmesi analizin temel sonuçlardan birisidir. İletim açıları eşit iken kaynak akımı ve doğrultucu akımı sıfır olmaktadır. Giriş voltajı ile çıkış voltajı arasındaki potansiyel farkın artması durumunda, açılar arasındaki fark da artmıştır. Ayrıca, süreksiz çalışma modunu belirleyen iletim açılarının sınır değerleri de verilmiştir.

Devrenin analiz edilmesi ve çalışma modunu belirlemek için gereken doğru parametre ayarlarını bulmak için PSpice programı kullanılarak önerilen doğrultucu devresinin simülasyonları gerçekleştirilmiştir. Karşılaştırma ve ek sonuçlar açısından aynı amaca yönelik olarak ayrıca MATLAB Simulink programı da kullanılmıştır. Önerilen doğrultucu devrenin simülasyonlarına yönelik gerçekçi ve tutarlı bir davranış elde edilmesi için iki farklı simülasyon yazılımı kullanılmıştır. Yapılan benzetimlerle devrenin kabul edilebilir giriş gerilimleri için sadece sürekli modda çalıştığı görülmüştür.

İletim açıları arasındaki ilişki, simülasyon sonuçlarından da elde edilmiş ve aralarında hemen hemen doğrusal bir ilişkinin olduğu gösterilmiştir. Devrede geniş bir iletim açısı değer aralığına ulaşmak için oldukça yüksek bir giriş gerilim genliğine ihtiyaç duyulmaktadır. Yapılan benzetimlerde iletim açılarının en geniş aralığının incelenmesi durumunda, elektrik devresinden çok yüksek bir akım akışı olacağı ortaya çıkmıştır. Bu akımı sağlamanın deneysel olarak mümkün olmayacağı görülmüştür. Gerçekleştirilen benzetimler ile edilen sonuçlar sayısal çözüm sonuçları ile birlikte çizdirilmiş ve mutlak yüzde hata oranı %14.4 olarak elde edilmiştir.

Elde edilen teorik sonuçlar ve benzetim karakteristiğinin doğrulanması için devrenin gerçekleştirilmesi yapılmıştır. Deneysel çalışmada değişen sinüzoidal gerilim genliği elde edilmesi için bir değişken transformatör (varyak) kullanılmıştır. Bunu daha hassas bir gerilim genliğinin doğrultucu sisteme sağlanmasını ve aynı zamanda devrenin topraktan izolasyonu sağlayan bir izolasyon transformatörü takip etmektedir. Varyak kullanılarak giriş gerilim genliğini gereksinim duyulan test koşulları için istenilen herhangi bir değere ayarlayabilmesi sağlanmıştır. Bu sayede devreden geçen elektrik akımı darbelerinin genliği değiştirilerek, mümkün olduğunca geniş bir iletim açısı aralığına ulaşılması sağlanmıştır.

Doğrultucu yapısı için kullanılan düzgülendirme indüktörü ve Schottky diyotlar, devreden geçen yüksek akım genliklerine uygun olarak seçilmiştir. Schottky diyotun tipik bir diyottan daha düşük bir ileri voltaj düşümü değerine sahip olması devre gerçekleştirilmesinde voltaj düşümünü azaltarak aynı zamanda toplam güç kaybını azaltılması açısından da yararlı bir özellik olarak ortaya çıkmıştır. Hedeflenen tasarım sabit bir gerilim yükü gerektirdiği için, çıkışta 12 V gerilime sahip, 12 Ah ve 9 Ah değerlerinde iki farklı kurşun-asit, sızdırmaz akü kullanılmıştır. Seçilen kurşun-asit pilin sabit yük olarak kullanılmasının uygun bir tercih olduğu yani bu çalışmadaki düşük iç dirençli dc kaynağın davranışını sağladığı elde edilen deneysel sonuçlarla gösterilmiştir.

12 Ah pil ile 9 Ah pilin aynı DC voltaj genliği ile beslendiklerinde 12 Ah pilin daha fazla akım çektiği tespit edilmiştir. Piller önemli ölçüde farklı akım çekmemekle birlikte, 12 Ah pilin küçük de olsa farklı akım değeri sağlaması, iletim açıları üzerinde ek hesaplamaya olanak sağlamıştır.

Gerçeklenen devrenin elektriksel ölçümleri için bir osiloskop kullanıldı. Osiloskopta akım ölçümleri için Hall etkisi sensör tabanlı bir akım probu kullanılmıştır. Kullanılan akım probunun kelepçe tipi yapısı ile test edilen devre üzerinde bağlantılar anlamında fiziksel değişiklik yapılmaya ihtiyaç olmadan okuma hassasiyeti yüksek bir ölçüm olanağı sağlanmıştır. Ölçüm cihazı olarak seçilen osiloskop için önemli olan diğer bir özellik, SCPI enstrümantasyon programlama ve kontrol alt yapısı olanağına sahip olmasıdır. MATLAB ortamında, hesaplama olanaklarının ve SCPI dilinin komutlarının birlikte kullanılması otomatik bir ölçüm sistemi programlamak için önemli olanaklar sağlamaktadır. Bu sayede gerçek ölçüm değerleri aynı ortamda sistematik biçimde elde edilerek bu çalışmada en temel noktalardan biri olan iletim açılarının hassas bir şekilde tespit edilmesini mümkün olmuştur.

MBR560 Schottky diyotunun seri direnci ( $r_s$ ), 42.15 m $\Omega$  olarak belirlenmiştir. Zaman sabiti yaklaşık olarak elektriksel periyodun %20'si olarak ortaya çıkmıştır. Simülasyonlar ile deneysel sonuçlar ve analitik model ile deneysel sonuçlar arasındaki sapmaları etkileyen temel faktörler, MBR560 Schottky diyotların sergilediği seri direnç ve doğrusal olmayan davranış özellikleridir.

Deneysel sistem kullanılarak elde edilen iletim açıları arasındaki ilişki de sunulmuş ve daha önceden verilen teorik yaklaşım ve benzetimlerle elde edilen sonuçların birbirini desteklediği gösterilmiştir. 12 Ah pil için giriş gerilim genliği 14.28 V olduğunda, sayısal çözüm ile deneysel bulgular arasındaki maksimum hata oranının %16,65 olduğu bulunmuştur. Simülasyon ve deneyden elde edilen iletimden çıkma açısı ( $\alpha_2$ ) değerleri sayısal çözümden elde edilen değerlerden daha küçük çıkmıştır. Devredeki yapılan modelde göz önünde bulundurulmayan dirençlerden kaynaklı  $I \cdot R$  gerilim düşümü etkisinin, devre akımının etkisiyle değeri değişen ters bağlı bir gerilim

kaynađı gibi davrandıđı, bu nedenle kaynak gerilimi deđerinin azalarak bunun sonucunun  $\alpha_2$  deđerlerini dűşürerek yansıdıđı görűlműştür.



## **1. INTRODUCTION**

### **1.1. Literature Review**

Rectifier circuits are essentially used in applications that require an AC to DC voltage conversion, such as power supplies and they have various configurations appearing in power electronics applications and research [1], [2].

Reviewing the literature shows that studies associated with single-phase full-wave rectifiers can be found for example in [3-12], and research that covers the three-phase rectifier topic is given in [13-23]. Studies of the rectifier's continuous conduction mode (CCM) can be found in [3],[4],[6] and the discontinuous conduction mode (DCM) was given in [5],[12],[20].

As for the rectifier circuit analysis and models, an analytical model of a diode bridge rectifier was presented in [9], an analytical model derived for a balanced, steady-state rectifier was given in [13],[14]. Yan D and Kwasinski presented a mathematical model of an uncontrolled rectifier circuit [8]. In [15], a numerical analysis of three-phase rectifier circuits was introduced. A rectifier's analytical expressions were given in [16], and a model of a rectifier with an electronic smoothing inductor (ESI) was proposed [17].

In [24], a novel approach for loop-cancelation technique in uncontrolled rectifier circuits was presented, an equivalent circuit of a single-phase diode rectifier was given in [10]. A differential model was proposed for analyzing Electromagnetic Interference (EMI) resulting from a single-phase rectifier [11], and analytical equations of a rectifier's steady-state operation were also introduced [12].

An estimated average model and control technique for a three-phase rectifier was given in [18]. An average model of a controlled rectifier was developed using state-space averaging techniques [20]. In [25], Q. Du, F. Meng, and L. Gao presented analytical formulas for the input current, power factor, and output current of a 12-pulse rectifier were introduced. Another example involves a study that offers a quantitative analysis of the operational characteristics of bridge rectifiers [26].

And about utilizing a smoothing inductor in the rectifier circuit, a series input inductor was added to a rectifier's input section in [3], and RL components were utilized as an input side filter in the rectifier circuit [4], also the impact of a smoothing inductor on the discontinuous mode was examined in another research [6]. In [17] ,[18], rectifiers with an Electronic Smoothing Inductor (ESI) were examined. Designing an input filter for a current source rectifier (CSR) based on the rectifier's allowed ripple in the input voltage was also given [27], a method for active damping on the oscillation of a rectifier's LC input filter was given in [19], a design of a passive filter for harmonic current is also presented [26].

Rectifiers supplying constant loads were also covered in the literature, as a single-phase uncontrolled rectifier circuit feeding a constant power load was presented by Yan D and Kwasinski [8], a rectifier having a constant DC voltage source as a load was presented in [14]. A three-phase constant voltage loaded rectifier circuit was given in [15], and a strategy that aims to mitigate the instability problems that result from constant power loads (CPLs) in rectifiers was given in [24].

The inclusion of a constant power load was examined with a single-phase diode rectifier [10]. Rectifiers with a constant voltage load in transient and steady-state situations are given in [26], and three-phase rectifiers with constant power loads (CPLs) on the DC bus are also presented in [22], so as a three-phase rectifier with a constant-voltage [23]. Examples of nonlinear load utilization were also given in [7], [13].

A technique of power factor correction in a rectifier was presented in [6], and in [16] mathematical formulas for the input power and power factor were presented. In [25], the development of an analytical formula for power factor was given, another research aimed to enhance the power quality of the circuit's power supply [5], the higher harmonics represented in power quality disturbances were discussed in [13], and enhancing power quality in power supply systems (UPS) is covered in [28].

The harmonics distortion in the AC input current of a three-phase rectifier was analyzed in [16], a model proposed to reduce the total harmonic distortion of the mains current was given in [17], the analysis of the presence of interharmonics and harmonics background distortion in the terminals' voltage of a single-phase diode bridge rectifier is presented in [9], also, an input filter design based on the rectifier's high-frequency

harmonic components in the grid current was introduced [27], and designing a passive filter for the harmonic current was given in [26].

## **1.2. Motivation of the Study**

When a rectifier operates in the discontinuous conduction operation mode (DCM), it means that the AC input current's waveform will experience intervals of current conduction and other zero-current intervals, which will result in the current waveform's having turn on and turn off angles, that vary depending on the circuit parameters [29].

The proper theoretical analysis of a rectifier requires developing an analytical model of it, and since rectifiers are nonlinear circuits [29], it is very hard to solve them analytically even when they are assumed to be using ideal diodes. Alternatively, analytical models for simplified versions of the rectifier circuits can be developed when the proper parameters and working conditions of the circuit are assumed.

This study presents the derivation of a rectifier circuit's analytical model. The circuit for which the analysis was made consists of a single-phase full-wave bridge rectifier circuit working in discontinuous conduction mode, a current-smoothing inductor at its input side, and a constant voltage load. The study investigates the nature of the relationship between the input current's conduction angles formed due to the discontinuous operation of the rectifier.

Besides the presentation of the theoretical results, supporting the study with several simulation test cases is important to examine how the rectifier circuit would operate with changes being made to the circuit's parameters. Also, the experimental circuit implementation was made and it gave results of the circuit performance, and how close are the theoretical results compared to the experimental results.

## **1.3. Content and Organization of the Thesis**

The thesis is organized in an order where it starts with the introduction in Chapter One, which includes presenting previous studies from the literature that have a common ground with this research, then an overview of the study and the motivation that influenced it.

Chapter Two, at the beginning, highlights some fundamental rectifier topologies and their benefits, then demonstrates the derivation of the analytical model, starting from the operation principles of the rectifier circuit, and then the necessary assumptions that were made to develop the model. Also, the results of the theory are presented and discussed in this chapter.

Chapter Three includes the circuit simulations that showcase the electrical characteristics of the proposed rectifier system for several test cases and how the change in the circuit's parameters affects them. The chapter also presents the relation between the conduction angles from the simulation result and compares it to the theoretical result.

In Chapter Four, the experimental circuit implementation is made and the necessary explanations for the component choices and software-related work are all introduced. The measurement results of the essential electrical characteristics are given and findings regarding the current conduction angles are also provided.

Chapter Five concludes the research.



## **2. ANALYTICAL MODEL AND RECTIFIER SYSTEM**

### **2.1. Contextual Framework**

After introducing some essential rectifier circuit topologies and their applications, this chapter presents the derivation of the proposed rectifier circuit's analytical model, then solve it and analyse its result. To execute this intent, the essential assumptions regarding the parameters of the model to be driven were made, and accordingly, the developed model that describes the relation between current's conduction angles was solved numerically using MATLAB and the solution's result was plotted to show the nature of relation between the targeted parameters of the final formula.

The single-phase full-wave bridge rectifier chosen for the development of the analytical model has a sinewave AC input voltage and at the input side of the rectifier circuit, a serial inductor was provided to the circuit to smooth the input current and the circuit was loaded with a constant voltage load. The formulas were driven by taking in to consideration that the rectifier is working in discontinuous conduction mode and steady state.

### **2.2. A Brief Overview of Diodes**

A diode is an electronic component that permits the flow of electrical current in one direction and has ideally infinite resistance to the current conduction in the other direction. Semiconductor diodes are the most common type of diode. The applied voltage polarity determines the conducting or cutting operations of a diode. By assuming the voltage source is greater than the diode's forward voltage ( $V_F$ ) rating, a diode acts as a closed switch when it has a forward bias connection to the voltage source and it acts as an open switch when it has a reverse bias connection to the voltage source. The typical forward voltage rating for a silicone diode is 0.7 V, which is the sufficient voltage drop across a diode to overcome the depletion region and conduct current [30].

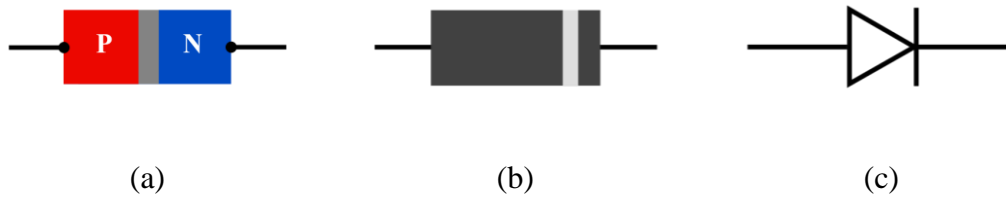


**Figure 2.1.** (a) The P-N junction, (b) Practical diode appearance, and (c) Diode symbol.

A Schottky diode is produced by utilizing metal contacted to a doped, n-type material of semiconductor, resulting in a metal-semiconductor junction that conducts current in forward biasing and acts as an open circuit reversely.

As can be seen in figure 2.2, the electrical characteristics of a Schottky diode show that it has a forward voltage drop lower than the typical diode, this feature is beneficial in terms of reducing the general voltage drop in the circuit design, hence, lower power loss. Besides that, a Schottky diode conducts current by electrons, resulting in a rather faster switching compared to the regular p-n junction diodes [31].

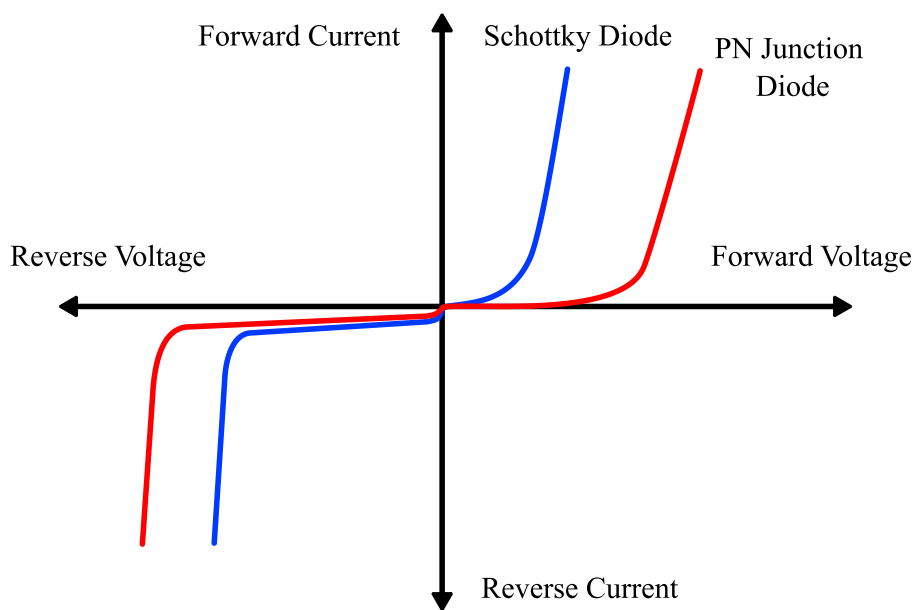


**Figure 2.2.** The voltage-current characteristics of a Schottky diode.

### 2.3. Rectifier Circuits

Rectification is the process of converting an alternating current signal (AC) into a direct current signal (DC), rectifiers are considered to be the most prevalent form of

diode applications, and rectifiers' working principle is based on the fundamental working principle of a diode.

The simplest model of a rectifier circuit is the half-wave rectifier, which consists of a voltage source, one forward-biased diode and a load. The main disadvantage of the half-wave rectification is that out of the full wave cycle, only half of it is supplied to the load which means inefficient utilization of the input voltage and that also makes it difficult to filter the DC output voltage due to the high harmonic content [1].

Full-wave rectification is also possible, an example of it is the centre-tapped full-wave rectifier and full-wave bridge rectifiers, their design allows the two half-cycles of the input voltage to pass and form a DC output voltage with complete-cycle conversion [1].

### 2.3.1. The full-wave bridge-rectifier circuit

The full-wave bridge rectifier utilizes four diodes and it rectifies the complete AC input voltage cycle on the contrary to the half-wave rectifiers. Figure 2.3 (a) shows the full wave rectifier with a resistive load. In the first semi-period of the AC voltage, diodes D1 and D4 conduct, which produces the first positive pulse of the output voltage, and diodes D2 and D3 conduct for the input's negative region. By conserving the polarity across the resistive load, the second positive pulse is produced [1], [30].

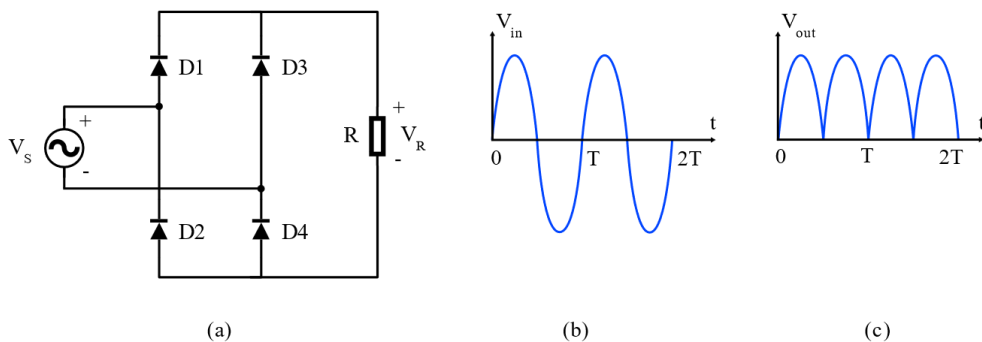


**Figure 2.3.** (a) Bridge-rectifier with resistive load, (b) AC input voltage, (c) Rectified output voltage.

Including a capacitor by a parallel connection to the output side of the rectifier circuit provides the circuit with a filtration function, as it reduces the ripple of the output voltage, as shown in figure 2.4. The beneficial characteristic of the capacitor is its ability to allow the alternating current (AC) signals to pass while it blocks the direct current (DC) signals [32].

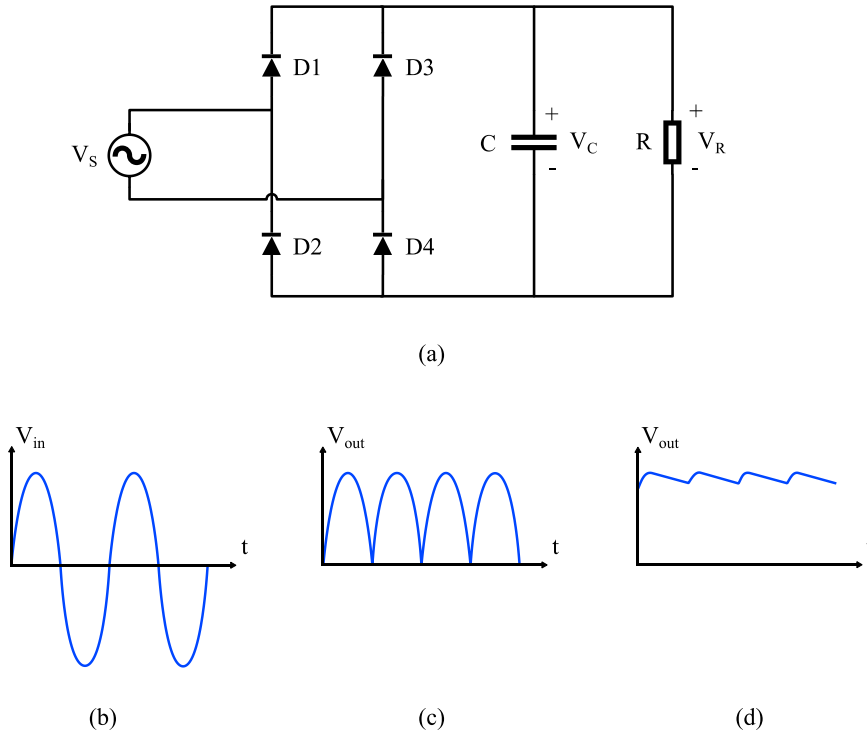


**Figure 2.4.** (a) Bridge-rectifier with capacitor filter and resistive load, (b) AC input voltage, (c) Rectified full-wave voltage, and (d) Capacitor-filtered DC output voltage.

### 2.3.2. Rectifier circuit with smoothing inductor and constant load

When the electrical current flows through a conductor wire, it produces a magnetic field surrounding that wire and that is the same situation with the inductor, which is simply a coil. When the current flows through an inductor, energy will be stored in the magnetic field surrounding it, which will become an energy source that restricts sudden changes, such as pulses in the current flowing through the inductor and this is the basic concept behind current smoothing or stabilization process. The current smoothing inductor can be used at the input or output side of the circuit as a filtering component [29].

In this thesis work, an inductor was used at the input side of the rectifier circuit to smooth the source current. Figure 2.5 shows a full-wave bridge-rectifier circuit with a current smoothing inductor at the AC input side having a constant voltage load once, and a resistive load with a capacitor filter on the other.

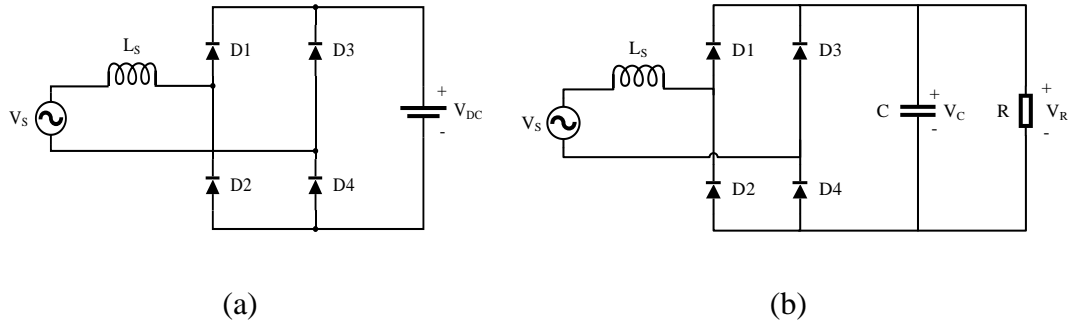


**Figure 2.5.** The rectifier circuit with a current smoothing inductor at the input side, (a) Feeding a constant voltage load, and (b) Feeding a resistive load with a capacitor filter.

### 2.4. Conduction Modes of the Rectifier

The rectifier operates either in continuous conduction mode (CCM) or discontinuous conduction mode (DCM). The current conduction occurs for most of the AC cycle in the continuous modes, whereas zero-current intervals of the current waveform happen in the case of discontinuous mode. And since the circuit topology in this research uses an inductor, the current was out of phase when compared to the voltage, so there was a phase shift between the input voltage and the input current, as the current lagged behind the voltage. Figure 2.6 shows the two operation modes.

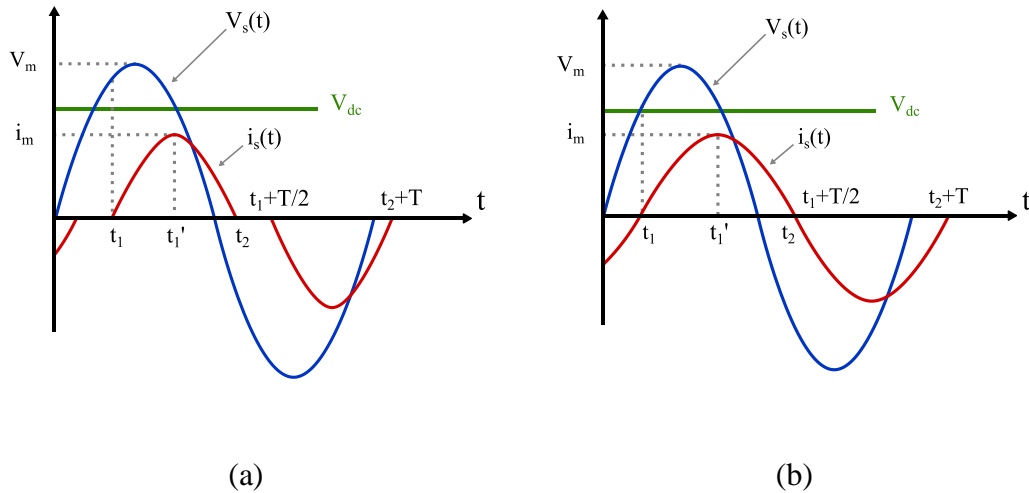


**Figure 2.6.** The AC source voltage and source current versus time for (a) The discontinuous conduction mode, and (b) The continuous conduction mode.

The rectifier circuit topology for which the analytical model was derived is shown in figure 2.7 (a). Figure 2.7 (b) shows the rectifier topology in case of feeding an RC

load. The equivalent circuits when the rectifier operates in continuous conduction mode and the diodes (D1 and D4, D2 and D3) do conduct are given in figure 2.8, and the equivalent circuits in case of the discontinuous conduction mode and diodes are not conducting are given in figure 2.9.

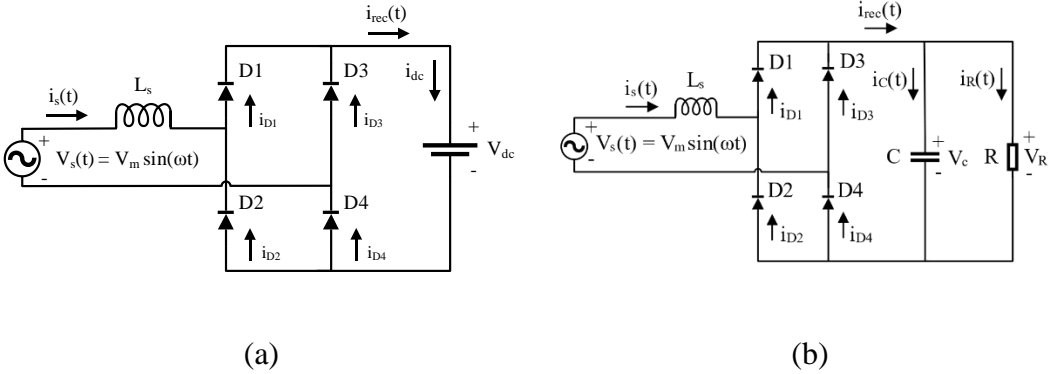


**Figure 2.7.** The rectifier circuit topology with an input smoothing inductor in case of (a) Feeding a battery load, and (b) Feeding an RC load.

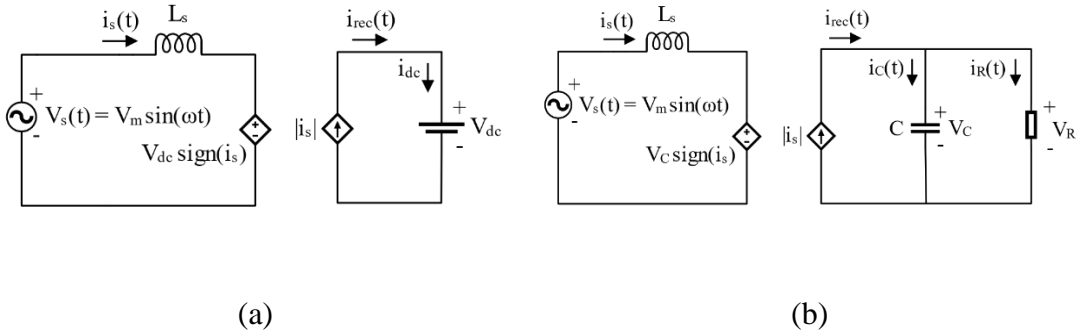


**Figure 2.8.** The equivalent circuit when diodes are conducting in case of (a) Feeding a battery load, and (b) Feeding an RC load.

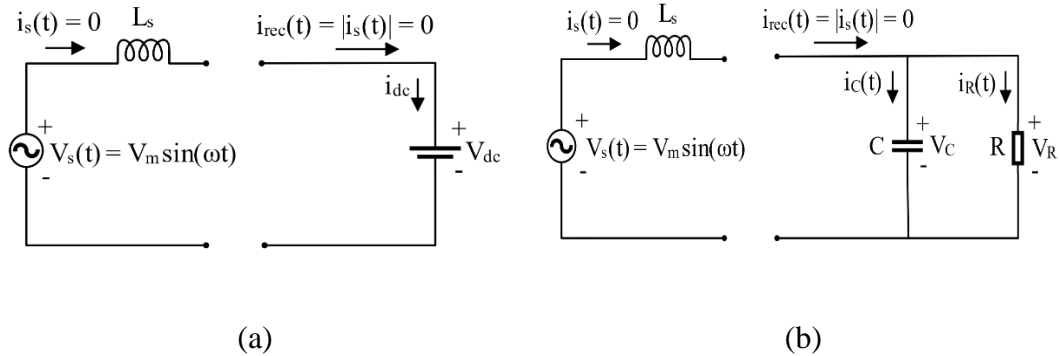


**Figure 2.9.** The equivalent circuit when diodes are not conducting with (a) A battery load, and (b) An RC load.

## 2.5. Derivation of the Steady State Analytical Model

To develop the analytical model, the following assumptions were considered [29]:

1. The source voltage waveform is sinusoidal.
2. The resistance of the smoothing inductor and its iron losses are negligible.
3. The inductance of the smoothing inductor is constant.
4. The DC output voltage is constant.
5. The diodes are ideal, their series resistance and threshold voltages are ignored.
6. The battery does not have an internal resistance, nor polarization capacitances and there are no series resistors connected with it.

Assuming that the circuit is operating in DCM, the sinusoidal source voltage can be given as:

$$V_s(t) = V_m \sin(\omega t) \quad (2.1)$$

Where  $V_s(t)$  is the source voltage,  $V_m$  is the amplitude of the input voltage,  $\omega$  is the angular frequency of the source and  $t$  is time.

When the diodes do conduct, the current of the rectifier is given as:

$$i_{rec}(t) = |i_s(t)| \quad (2.2)$$

Where  $i_s(t)$  represents the source current.

At  $t=t_1$ , the diodes D1 and D4 start to conduct, when the source voltage is the same as the DC output voltage:

$$V_s(t_1) = V_m \sin(\omega t_1) = V_m \sin(\alpha_1) = V_{dc} \quad (2.3)$$

Where  $\alpha_1 = \omega t_1$  represents the turn on angle when  $t=t_1$ , it is given as:

$$\alpha_1 = \arcsin(V_{dc}/V_m) \quad (2.4)$$

The value of angle  $\alpha_1$  should be between 0 and  $\pi/2$ . In the case of  $V_{dc} \geq V_m$ , there will be no conduction. When two diodes do conduct and taking into consideration the equivalent circuit in figure 2.8:

$$V_s(t) = V_m \sin(\omega t) = L_s \frac{di_s}{dt} + \text{sign}(i_s)V_{dc} \quad (2.5)$$

Where  $L_s$  is the smoothing inductor's inductance.

Having diodes D1 and D4 conducting and assuming that the output voltage is constant, the source current is positive, equation 2.5 can be solved by taking each side's integral with respect to time:

$$\int_{t_1}^t V_m \sin(\omega t) dt = \int_{t_1}^t L_s \frac{di_s}{dt} dt + \int_{t_1}^t V_{dc} dt \quad (2.6)$$

$$-\frac{V_m}{\omega} (\cos(\omega t) - \cos(\omega t_1)) = L_s (i_s(t) - i_s(t_1)) + V_{dc}(t - t_1) \quad (2.7)$$

After rearranging equation 2.7, it is possible to obtain the source current as:

$$i_s(t) = \frac{1}{\omega L_s} (V_m (\cos \alpha_1 - \cos(\omega t)) - V_{dc} \omega (t - t_1)) \quad (2.8)$$

Considering the electrical angle as  $\alpha = \omega t$ , the equation 2.8 becomes:

$$i_s(\alpha) = \frac{1}{\omega L_s} (V_m (\cos \alpha_1 - \cos(\alpha)) - V_{dc} (\alpha - \alpha_1)) = \frac{V_m f(\alpha)}{\omega L_s} \quad (2.9)$$

As was given in equation 2.9, the source current ( $i_s$ ) is dependent on the function  $f(\alpha)$ , which is equal to:

$$f(\alpha) = \cos \alpha_1 - \cos \alpha + \sin \alpha_1 (\alpha - \alpha_2) \quad (2.10)$$

For  $t = t_2$ , or  $\alpha = \alpha_2$ , the source current or  $f(\alpha)$  turns to zero, as shown in figure 2.6 (a):

$$i_s(\alpha_2) = \frac{1}{\omega L_s} (V_m (\cos \alpha_1 - \cos \alpha_2) - V_{dc} (\alpha_2 - \alpha_1)) = 0 \quad (2.11)$$

$$f(\alpha_2) = \cos \alpha_1 - \cos \alpha_2 + \sin \alpha_1 (\alpha_1 - \alpha_2) = 0 \quad (2.12)$$

To calculate time values corresponding to the angles at which conduction begins and stops, the formulas are given as:



$$t_1 = \frac{\alpha_1}{\omega} \quad (2.13)$$

And

$$t_2 = \frac{\alpha_2}{\omega} \quad (2.14)$$

Equation 2.12 is nonlinear and cannot be solved analytically, but it can be solved numerically. The turn off angle ( $\alpha_2$ ) is to be solved by having the turn on angle ( $\alpha_1$ ) values vary from 0 to  $\pi/2$ . MATLAB was used to solve equation 2.12 numerically [33]. The  $\alpha_2$  as a function of  $\alpha_1$  is plotted in figure 2.10. Since the resulting plot is almost linear, the relationship between the conduction angles,  $\alpha_1$  and  $\alpha_2$ , can be expressed as:

$$\alpha_2 = m_{\text{fit}}\alpha_1 + n_{\text{fit}} \quad (2.15)$$

It is possible to use the least squares method to obtain  $m_{\text{fit}}$  and  $n_{\text{fit}}$  values, the solution is almost a line. The curve fitter tool in MATLAB was used for the numerical solution, for the range of  $\alpha_1$  between  $32.4816^\circ$  to  $90^\circ$  [34], the following values were obtained:

$$m_{\text{fit}} = -2.1123 \quad (2.16)$$

And

$$n_{\text{fit}} = 4.8625 \quad (2.17)$$

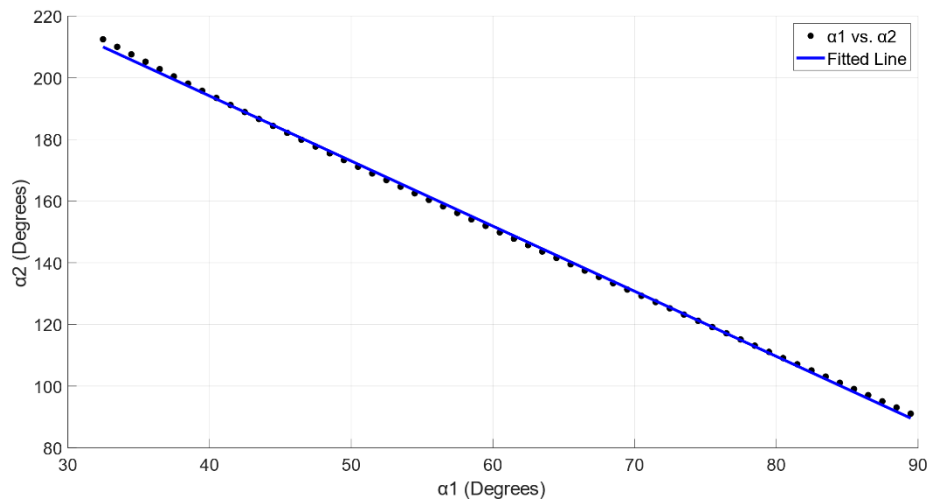


**Figure 2.10.** The numerical solution result and the curve fitting for  $\alpha_1$  vs.  $\alpha_2$ .

Since solving equation 2.12 resulted in an almost a line plot, that equation can be considered as almost linear, an equation of line with two-point (right and left) boundaries can be found, to give an approximated line plot. In case of not having conduction, the angles of the zero-load can be found as:

$$\alpha_1 = \alpha_2 = \alpha_{\text{critic}} = \pi/2 \quad (2.18)$$

In case of the rectifier is operating in the continuous conduction mode, then:

$$\alpha_2 = \alpha_1 + \pi \quad (2.19)$$

For this case:

$$\cos \alpha_1 - \cos(\alpha_1 + \pi) + \sin \alpha_1 (\alpha_1 - (\alpha_1 + \pi)) = 0 \quad (2.20)$$

$$\cos \alpha_1 + \cos(\alpha_1) - \sin \alpha_1 \pi = 0 \quad (2.21)$$

$$2\cos \alpha_1 - \sin \alpha_1 \pi = 0 \quad (2.22)$$

$$2\cos \alpha_1 = \sin \alpha_1 \pi \quad (2.23)$$

$$\frac{\sin \alpha_1}{\cos \alpha_1} = \tan \alpha_1 = \frac{2}{\pi} \quad (2.24)$$

$$\alpha_1 = \arctan\left(\frac{2}{\pi}\right) = 32.4816^\circ \quad (2.25)$$

Returning to equation 2.4, the rectifier's CCM operation starts if  $V_m = V_{dc}/\sin(32.4816^\circ)$  and it keeps operating in CCM for  $\alpha_1 \leq 32.4816^\circ$ .

For the continuous conduction mode, time  $t_1$  can be found as:

$$t_1 = \frac{\alpha_1}{\omega} = \frac{\arctan\left(\frac{2}{\pi}\right)}{\omega} \quad (2.26)$$

And the angle  $\alpha_2$  can be found as:

$$\alpha_2 = \arctan\left(\frac{2}{\pi}\right) + \pi \quad (2.27)$$

And the time  $t_2$  can be found as:

$$t_2 = t_1 + T/2 = \frac{\arctan\left(\frac{2}{\pi}\right)}{\omega} + T/2 \quad (2.28)$$

Where  $T=1/f$  represents the electrical period of one complete wave cycle of the source voltage and  $f$  is the source frequency.

The line tangent approximation can use the start angles of continuous conduction mode and the zero-load angles to find:

$$m = \frac{\pi/2 - (\arctan\left(\frac{2}{\pi}\right) + \pi)}{\pi/2 - \arctan\left(\frac{2}{\pi}\right)} = -\frac{(\arctan\left(\frac{2}{\pi}\right) + \pi/2)}{\pi/2 - \arctan\left(\frac{2}{\pi}\right)} \quad (2.29)$$

And

$$n = \pi/2 - m \cdot \pi/2 = \frac{\pi}{\pi/2 - \arctan\left(\frac{2}{\pi}\right)} \quad (2.30)$$

Calculating the equation of the line's parameters using equation 2.29 and equation 2.30 results in the values of  $m = -2.1294$  and  $n = 4.9157$ . The two values can be substituted in the equation of the line for the range of  $\alpha_1$  from  $32.4816^\circ$  to  $90^\circ$ , and the result is plotted in an approximated line, as shown in figure 2.11.

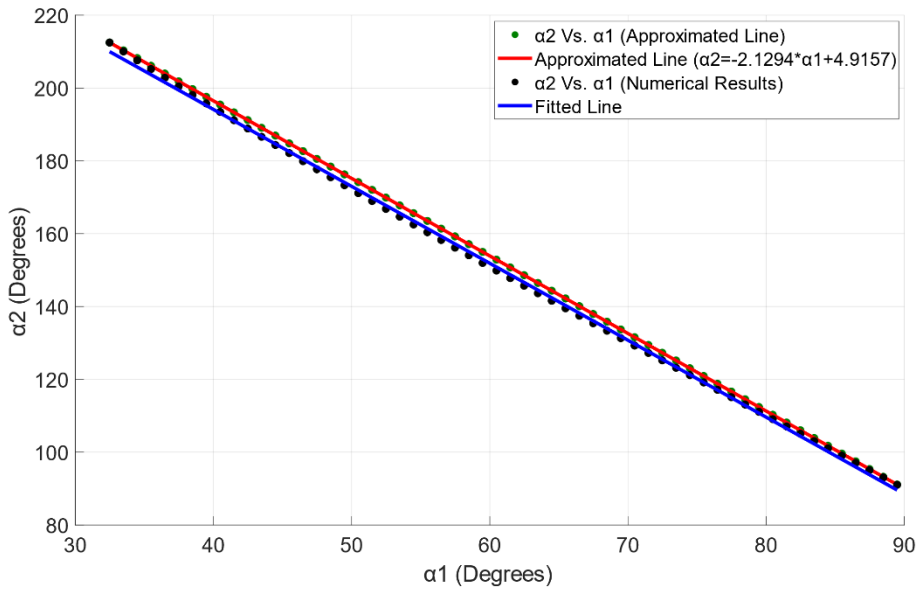


**Figure 2.11.**  $\alpha_1$  vs.  $\alpha_2$  for both the numerical result with the linear regression and approximated line.

The nature of the relation between  $\alpha_1$  and  $\alpha_2$  in accordance with the input voltage amplitude is given in figure 2.12.

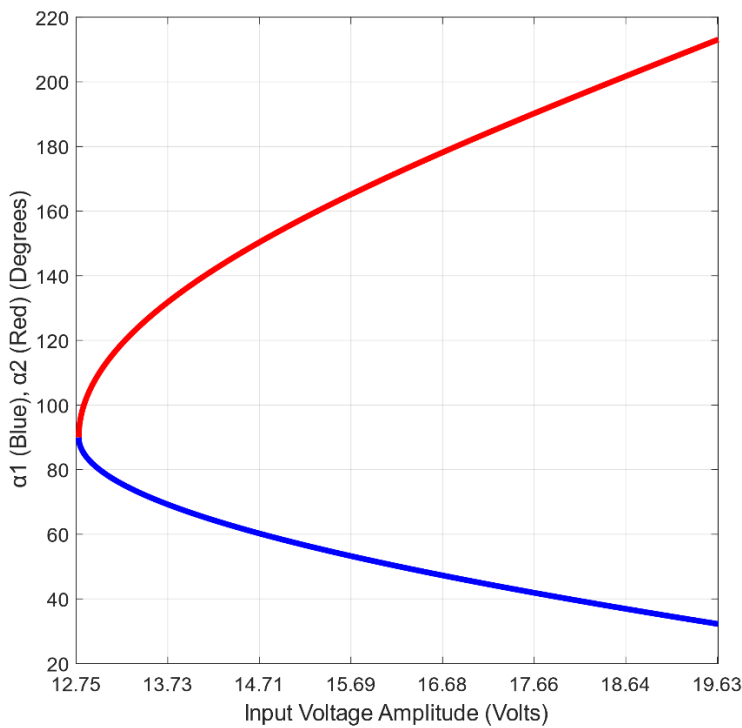


**Figure 2.12.** The complementary relation between the conduction angles ( $\alpha_1$  and  $\alpha_2$ ) and the input voltage amplitude.

The complementary behaviour of the conduction angles can be noticed in the previous figure 2.12. When the input voltage amplitude equals the DC output voltage, there will be no current conduction, the  $\alpha_1$  and  $\alpha_2$  will meet at  $90^\circ$ , while in case of increasing the potential difference between the input voltage and the output voltage, the divergence between the two conduction angles will also increase, in this case, it is given for  $\alpha_1$  values between  $32.4816^\circ$  and  $90^\circ$ .

And the nature of the relation between the normalized value of the DC output voltage by the peak input voltage ( $V_{dc}/V_m$ ), ranging from  $\sin(\arctan(2/\pi))$  to 1 and both the turn on angle ( $\alpha_1$ ) and the turn off angle ( $\alpha_2$ ) is given in figure 2.13.

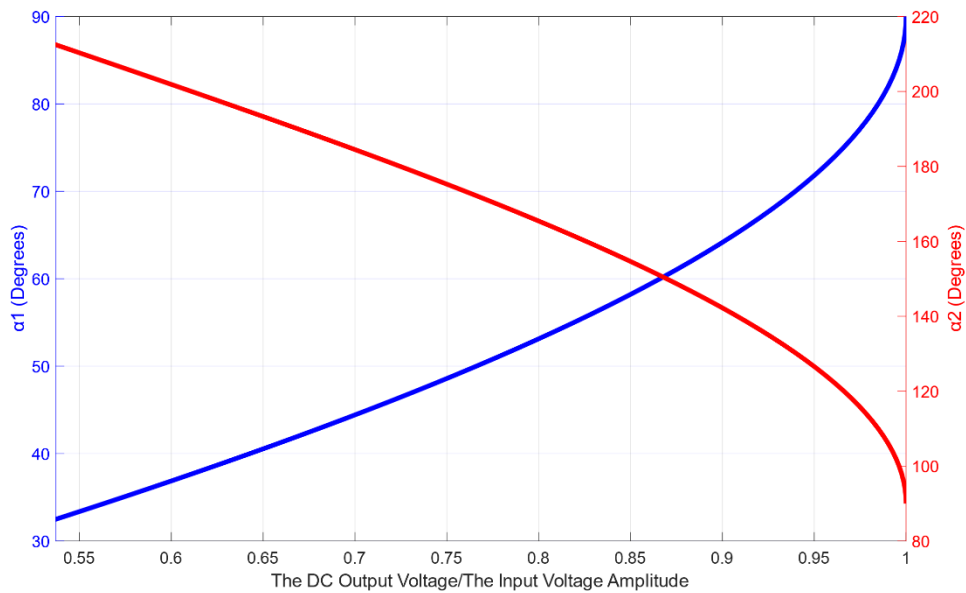


**Figure 2.13.** The complementary relation of the plots of  $\alpha_2$  vs.  $V_{dc}/V_m$  and  $\alpha_1$  vs.  $V_{dc}/V_m$ .



### **3. SIMULATION OF THE RECTIFIER SYSTEM**

#### **3.1. The Electrical Characteristics of the Rectifier System**

Simulations were done to examine the main electrical characteristics of the circuit in this research, which includes the input current working in discontinuous conduction mode (DCM) and the constant output voltage, besides examining the input voltage amplitude at which the continuous conduction mode can be achieved and checking the effect of varying the amplitude of the input voltage on the input current's waveform was important because it enabled the analysis of the relation between the conduction angles, which was given at the end of this chapter.

To ensure that accurate simulation results are obtained and a constant behaviour for the fundamental simulations of the proposed rectifier circuit is achieved, two simulation software were used, OrCAD's PSpice and the MATLAB-integrated, Simulink.

#### **3.2. Simulation Results of PSpice**

From the OrCAD suite, OrCAD Capture was used to draw the schematics of the rectifier circuit, the software also allows the placement of probes to the desired nodes for voltage or branch current to be simulated. Then PSpice simulated the circuit to display the electrical characteristics of desired voltages and currents, with its simulation interface [35], [36].

The schematic of the full-wave bridge rectifier circuit in OrCAD Capture software is shown in figure 3.1. A sinusoidal voltage source was used to supply the circuit with AC input voltage, operating at 50 Hz of frequency. The input-current smoothing inductor, which has 330  $\mu\text{H}$  inductance value is placed at the input side of the bridge rectifier, also, the rectifier circuit feeds a constant voltage load, where a DC voltage source was used, its value was chosen as 12.75 V. Also, a Schottky diode, with the model number SB30-03F was used for the bridge rectifier, it was originally set to have 0.39 V of forward voltage by the software developer, then it was adjusted to 0.4 V for

this research’s simulations, where parameters changing is possible in OrCAD Capture, to bring it closer to the experimentally used diode model which has 0.4 V of forward voltage rating given in its datasheet. The SB30-03F diode’s internal resistance is 42.14 mΩ. The low forward voltage of the Schottky diode plays an important role in reducing the overall voltage drop in the circuit, which reduces the error rate between the turn on and turn off angles when the numerical and simulation results are compared to each other.

A resistor with a small resistance value of 1 mΩ was needed to be connected in series with the constant load to avoid oscillations with high frequency from being present in the output voltage waveform, arising from the diodes’ junction capacitances and the input smoothing inductor.

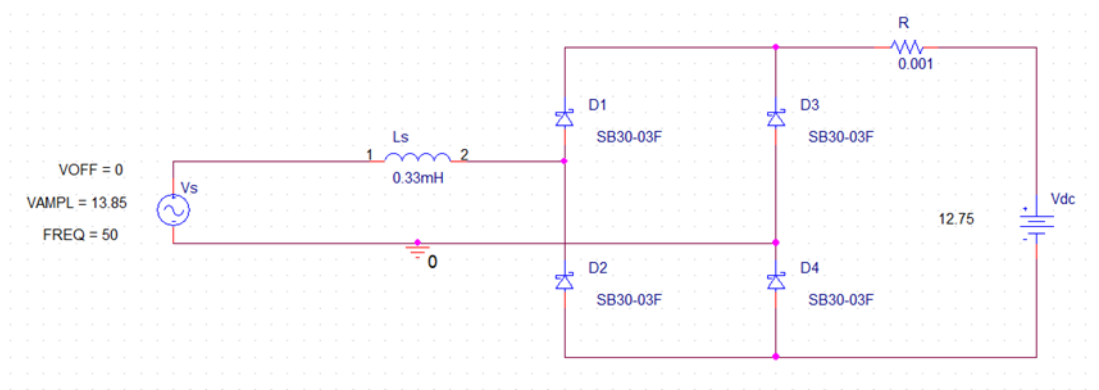


**Figure 3.1.** The rectifier circuit schematic in OrCAD Capture.

For the first simulation test case, the amplitude of the input voltage was set to 13.85 V, and by having the DC load voltage as 12.75 V, there was a 1.1 V of potential difference between the input and the output voltages, about 1.03 A of current flowed through the circuit as can be seen in figure 3.2 (b).

It can also be seen in figure 3.2 (b) that the input current’s waveform starts with a time interval having a zero current amplitude, resulting from the input voltage not reaching the diode’s forward voltage threshold yet, when it does, the rectifier will be working in Discontinuous Conduction Mode, so the angles at which the current conduction starts and stops, which are called turn on and turn off angles are affected by diode’s forward voltage and the battery’s voltage value, that define the time interval at which the conduction starts for each half cycle. When the diode has a lower forward voltage, the current conduction can occur at an earlier time, the rectifier has two diodes working for each half cycle, making the considered forward voltage which is required for the



current conduction to occur as the summation of two diodes' forward voltages, so 0.8V.

When the conduction occurs, the current waveform will appear like a plus having a triangular-like waveform, the usage of an input current smoothing inductor, which stores energy as a magnetic field, resulting in the input current's waveform not having a sharp falling slope, but gradual, when the input voltage decreases beyond the diodes' forward voltage for each half cycle. Figure 3.3 (a) shows the output voltage, which also has a pulsative nature. When there is no current conduction, the output voltage's waveform will show an interval with only the battery's terminal voltage amplitude, when current conduction happens, there will be a voltage drop across the series-connected resistor, and due to the pulsative nature of the current, the output voltage of the circuit, which is given by  $V_{out}=i_{rec}(t)R+V_{dc}$ , will also show these pulsed ripples. The output voltage's ripple was only about 1 mV in this simulation case.

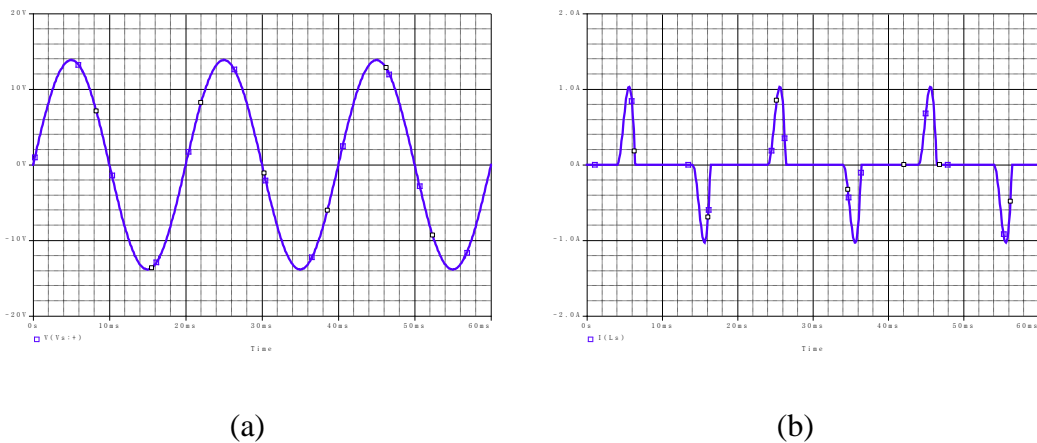


**Figure 3.2.** Simulation result of PSpice for (a) Input voltage, and (b) Input current.

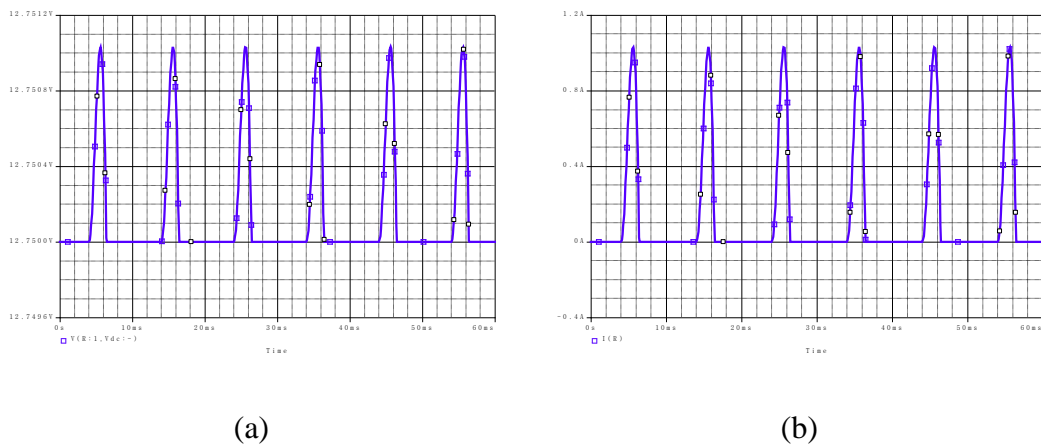


**Figure 3.3.** Simulation result of PSpice for (a) Output voltage, and (b) Output current.

### 3.2.1. Reducing the smoothing inductor's inductance

More PSpice simulation cases can be given, where the parameters of the circuit are changed to check the impact of that change on the circuit's characteristics, as the voltage and current amplitudes and waveforms can change, due to the change in the circuit's parameters.

One example of parameter change is where the inductance of the input current's smoothing inductor is reduced from 330  $\mu\text{H}$  to 50  $\mu\text{H}$ , while keeping the input voltage amplitude as 13.85 V and the constant load's voltage as 12.75 V. That reduction in the inductor's inductance allowed about 2.46 A of current to flow through the circuit and the ripple of the DC output voltage was about 2.5 mV. The rectifier circuit kept working in discontinuous conduction mode. As it can be seen in figure 3.4 and figure 3.5 there was not a significant change in the waveforms, especially regarding the input current and the output voltage.

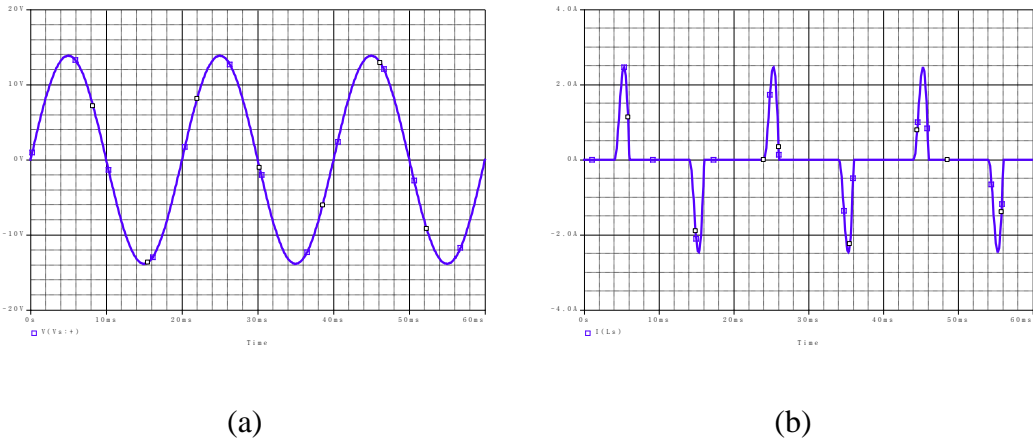


**Figure 3.4.** Simulation results for (a) The input voltage, and (b) The input current when the smoothing inductor's inductance is reduced to 50  $\mu\text{H}$ .

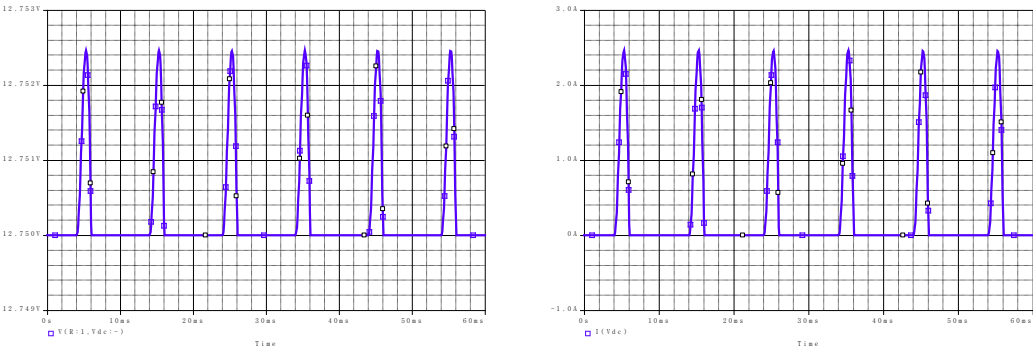


**Figure 3.5.** Simulation results for (a) The output voltage, and (b) The output current when the smoothing inductor's inductance is reduced to 50  $\mu\text{H}$ .

### 3.2.2. The continuous conduction mode

Increasing the input voltage amplitude is the main parameter change that can be done to the rectifier circuit to make it operate in the continuous conduction mode. Since the analytical model introduced in the second chapter predicted that the continuous conduction mode would start when the input voltage amplitude exceeds 19.63 V, the first CCM simulation test case is given with a higher input voltage amplitude than this prediction value. The smoothing inductor's inductance was returned to 330  $\mu\text{H}$ .

The first CCM simulation test case was made with the input voltage amplitude set to 25 V and both the output voltage and the smoothing inductor's inductance were kept the same as in the previous test cases. The rectifier kept working in the discontinuous conduction mode, as can be seen in figure 3.6 (b), The current amplitude reached 75.9 A, and the ripple in the output voltage was 7.5 mV. Both figure 3.6 and figure 3.7 show this simulation case.

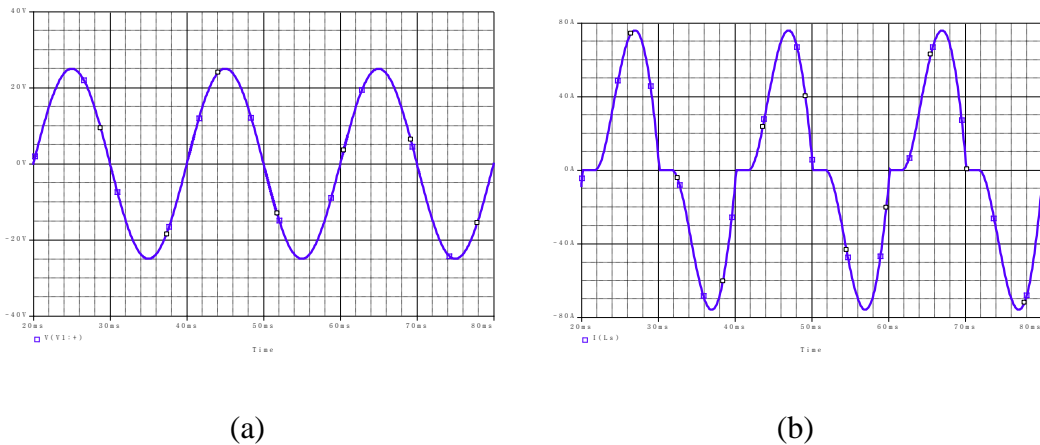


**Figure 3.6.** (a) The input voltage, and (b) The input current, when  $V_m = 25$  V.

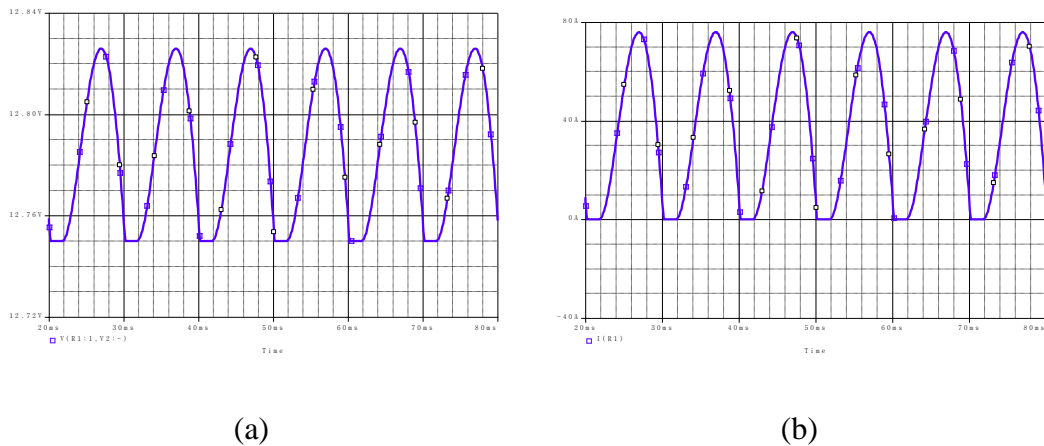


**Figure 3.7.** (a) The output voltage, and (b) The output current, when  $V_m = 25$  V.

The next test case was made to examine the possibility of CCM occurrence with input voltage amplitude being  $V_m = 40\text{ V}$ , while keeping all the other parameters the same, unfortunately, neither that case made the rectifier reach a full CCM, and didn't follow the analytical model prediction regarding this mode, as can be seen in figure 3.8 and figure 3.9. The current reached an amplitude of 195 A, and the output voltage's ripple was 195 mV.

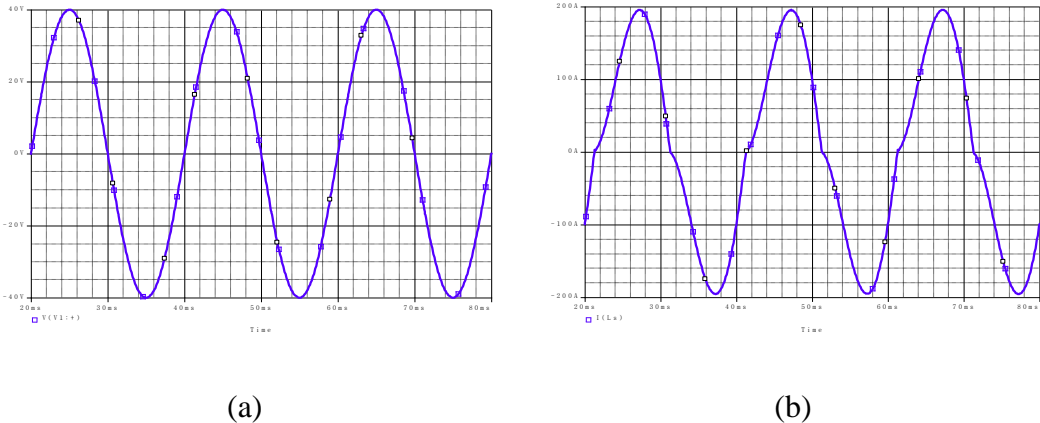


**Figure 3.8.** (a) The input voltage, and (b) The input current, when  $V_m = 40\text{ V}$ .

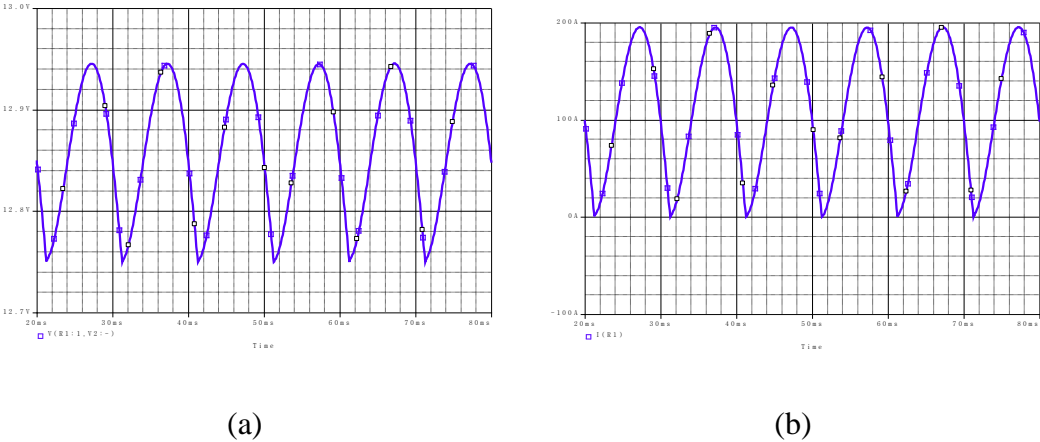


**Figure 3.9.** (a) The output voltage, and (b) The output current, when  $V_m = 40\text{ V}$ .

### 3.3. Simulation Results of Simulink

MATLAB was used to perform several tasks in this research, including its integrated companion, Simulink, where Simulink's environment provides a block-based tool for circuit modelling, which offers convenient simulation abilities and a large library of element options [33]. The essential electrical simulations of the rectifier circuit were carried out using Simulink.

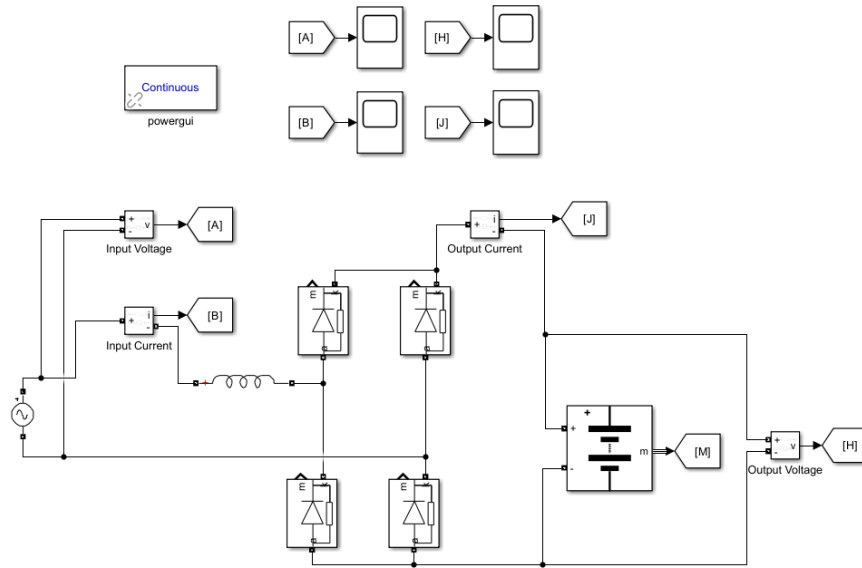
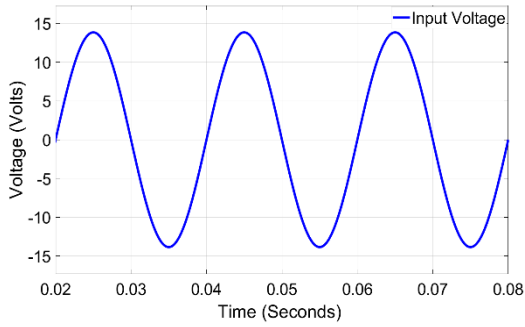
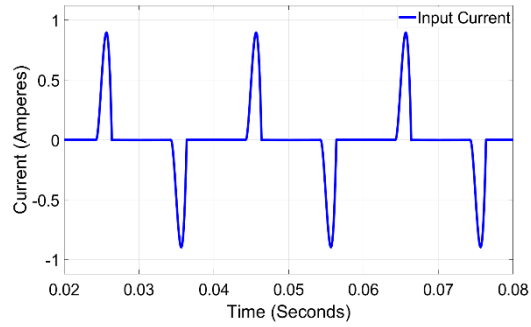


**Figure 3.10.** Block diagram of the rectifier circuit drawn in Simulink.

The diode's parameters in the Simulink model were adjusted similarly to the parameters available in OrCAD Capture's diode model, where the diode's internal resistance was made to be 42 mΩ and the forward voltage was made to 0.4 V. A sinusoidal voltage source was used to supply the circuit with the input voltage at 50 Hz of operational frequency. The battery's voltage value was also adjusted to 12.75 V. The first simulation made with Simulink is given in figure 3.11 and figure 3.12, in this test case, the input voltage amplitude was 13.85 V, which allowed 0.9 A of current to flow through the circuit, it can also be noticed that the input current in Simulink's simulation result shows a very similar waveform and amplitude compared to PSpice's results, where the tringle-like current waveform is also present here in each half cycle, with the zero current intervals at the beginning and end of the period, so the descriptions of the older PSpice's results are valid here. The output voltage's ripple was about 1 mV in this case.

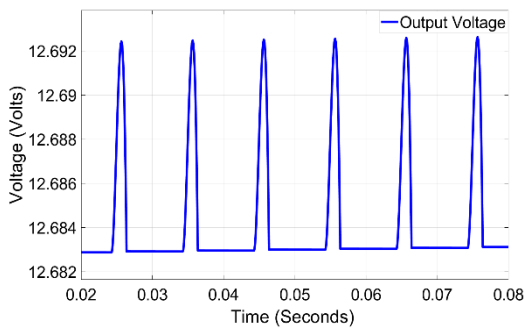


(a)

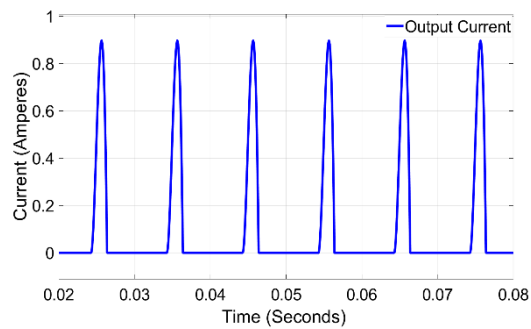


(b)

**Figure 3.11.** Simulation result of Simulink for (a) Input voltage, and (b) Input current.



(a)



(b)

**Figure 3.12.** Simulation result of Simulink for (a) Output voltage, and (b) Output current.

### 3.3.1. Reducing the smoothing inductor's inductance

In this test case, all the circuit parameters are kept the same, but the smoothing inductor's inductance was reduced to 50  $\mu\text{H}$ , the main difference that can be noticed due to this change is the increase of the input current amplitude from 0.9 A of the previous test to 2.73 A. It can also be noticed that the ripple of the DC output voltage is about 3 mV in this testing case. Figure 3.13 and figure 3.14 show this simulation case.

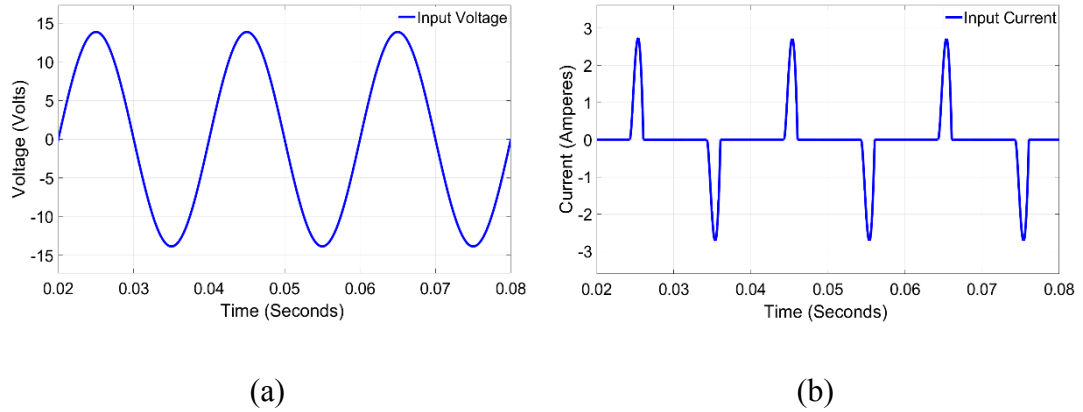


**Figure 3.13.** Simulation results for (a) The input voltage, and (b) The input current when the smoothing inductor's inductance is adjusted to 50  $\mu\text{H}$ .

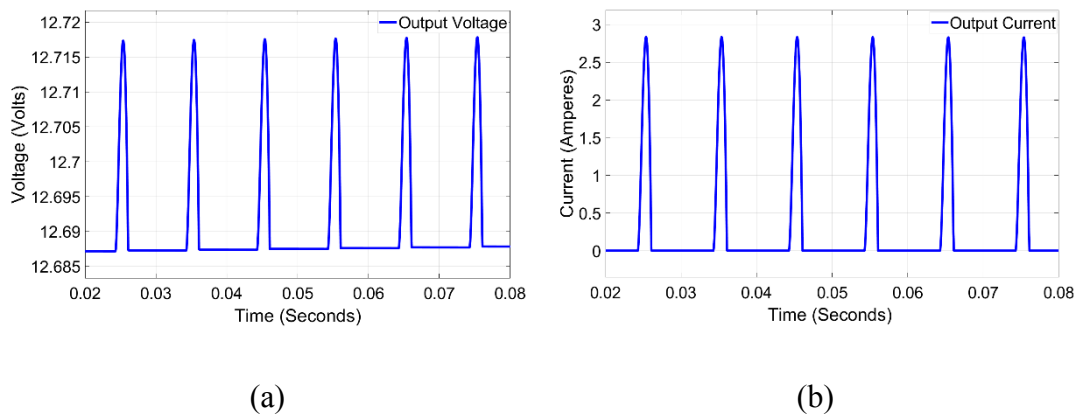
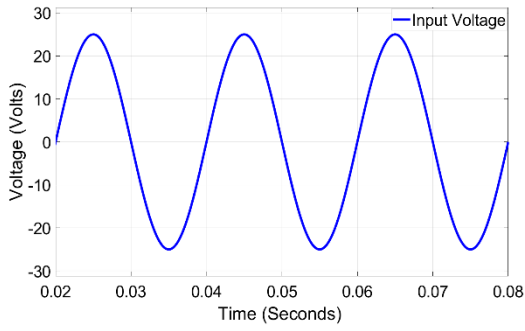


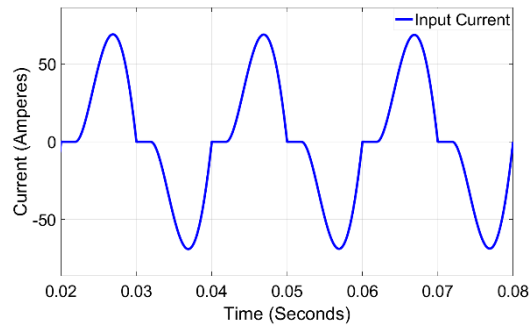
**Figure 3.14.** Simulation results for (a) The output voltage, and (b) The output current when the smoothing inductor's inductance is adjusted to 50  $\mu\text{H}$ .

### 3.3.2. The continuous conduction mode

The continuous conduction mode was attempted in Simulink as it was in PSpice, by increasing the input voltage amplitude to 25 V while keeping all the other parameters the same, which includes returning the smoothing inductor's inductance to 330  $\mu\text{H}$ . As the case was with PSpice, the circuit didn't operate in CCM when  $V_m = 25$  V, the current amplitude was 69 A and the output voltage's ripple was 790 mV. This simulation case's results are shown in figure 3.15 and figure 3.16.

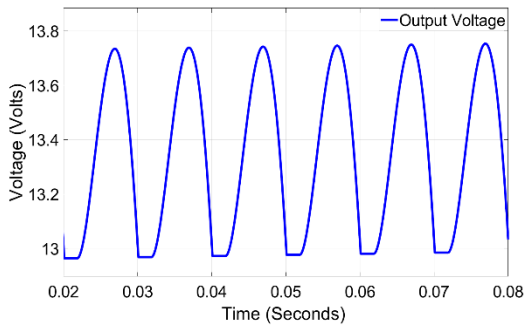


(a)

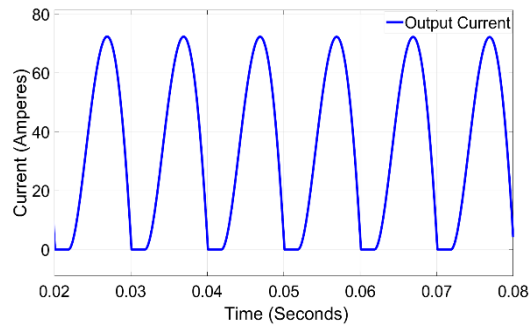


(b)

**Figure 3.15.** Simulation result of (a) Input voltage, and (b) Input current when  $V_m=25V$ .



(a)



(b)

**Figure 3.16.** Simulation result of (a) Output voltage, and (b) Output current when  $V_m=25 V$ .

The following simulation case was made after increasing the input voltage amplitude to 40 V while keeping all the other parameters the same, the circuit didn't operate in a full CCM when  $V_m=40 V$ , the current amplitude was 182 A and the output voltage's ripple was 194 mV. This simulation case's results are shown in figure 3.17 and figure 3.18.



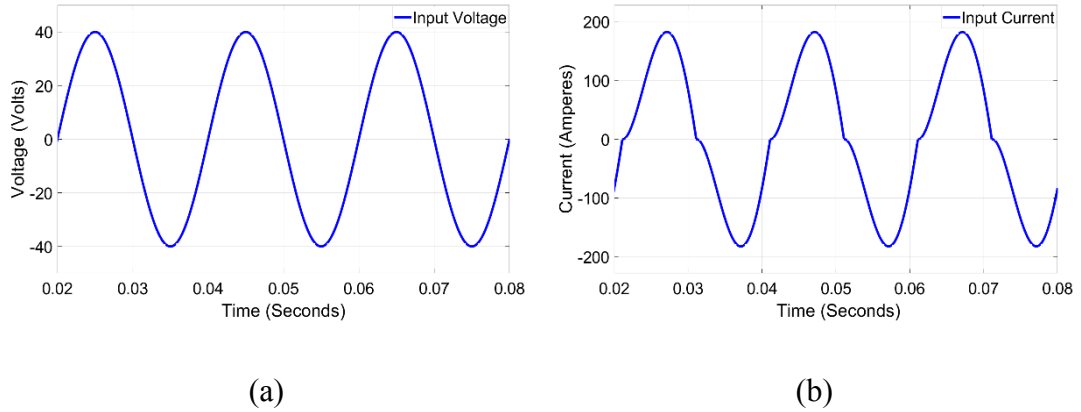


**Figure 3.17.** Simulation result of (a) Input voltage, and (b) Input current when  $V_m=40V$ .

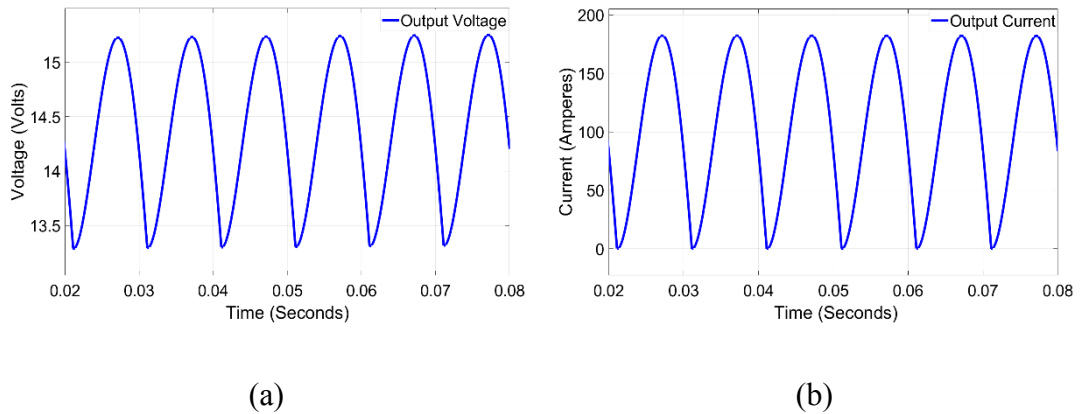


**Figure 3.18.** Simulation result of (a) Output voltage, and (b) Output current when  $V_m=40 V$ .

### 3.4. The Relation Between the Conduction Angles

To examine the relation between the turn on and turn off angles obtained from simulation results and compare it to the numerical results and to calculate the error between the two results, a total of 22 cross points of  $\alpha_1$  versus  $\alpha_2$  were calculated from the circuit's simulation in the PSpice program and 20 cross points were calculated from Simulink, when the rectifier was operating in discontinuous mode.

The first simulation test was made to achieve a turn on angle near  $\alpha_1 = 23^\circ$ , which required an input voltage amplitude of 40 V for both simulation software. The last calculated value of the turn on angle was  $\alpha_1 = 81^\circ$  for PSpice, for which the circuit was supplied with 12.9 V of input voltage amplitude. For Simulink, the highest obtained turn on angle value was  $\alpha_1 = 86.4^\circ$  when the circuit was supplied with 13.25 V of input voltage amplitude, no further calculation (a higher  $\alpha_1$  value for PSpice and Simulink)

was possible due to the minimum current amplitude and the non-uniform current waveform.

The calculation of the conduction angles was made as follows. The turn on ( $\alpha_1$ ) angle was calculated by multiplying the time at which the conduction starts ( $t_1$ ) by the angular frequency ( $\omega$ ), using equation 3.1, and the turn off angle ( $\alpha_2$ ) was calculated by multiplying the time at which the conduction stops ( $t_2$ ) by the angular frequency ( $\omega$ ) using equation 3.2.

$$\alpha_1 = \omega t_1 \quad (3.1)$$

$$\alpha_2 = \omega t_2 \quad (3.2)$$

Figure 3.19 shows the relation between the conduction angles calculated from the simulation and the numerical results, where the range of turn on angle values for the simulation result was between  $23^\circ$  to  $86.4^\circ$  and the numerical result of ( $\alpha_1$ ) was between  $23^\circ$  to  $90^\circ$ .

The absolute percentage error between the numerical result and the simulation result for each value of the turn off angle ( $\alpha_2$ ) was calculated using equation 3.3.

$$APE = \left| \frac{F - A}{A} \right| \times 100 \quad (3.3)$$

Where F represents the forecasted or estimated value, which is the simulation value in this case, and A represents the numerical result. When the turn on ( $\alpha_1$ ) angle was  $\alpha_1 = 23^\circ$ , the calculated absolute percentage error between the numerical solution's turn off angle ( $\alpha_2$ ) and the PSpice's turn off ( $\alpha_2$ ) angle was 14.27% and it was 14.4% when the numerical  $\alpha_2$  result was compared to Simulink's  $\alpha_2$  result.

And when the turn on ( $\alpha_1$ ) angle was  $\alpha_1 = 86.4^\circ$ , the absolute percentage error between the numerical solution's turn off angle ( $\alpha_2$ ) and the Simulink's turn off ( $\alpha_2$ ) angle was 1.2%, when  $\alpha_1 = 81^\circ$ , it was 6.32% when the numerical  $\alpha_2$  result was compared to PSpice's  $\alpha_2$  result.

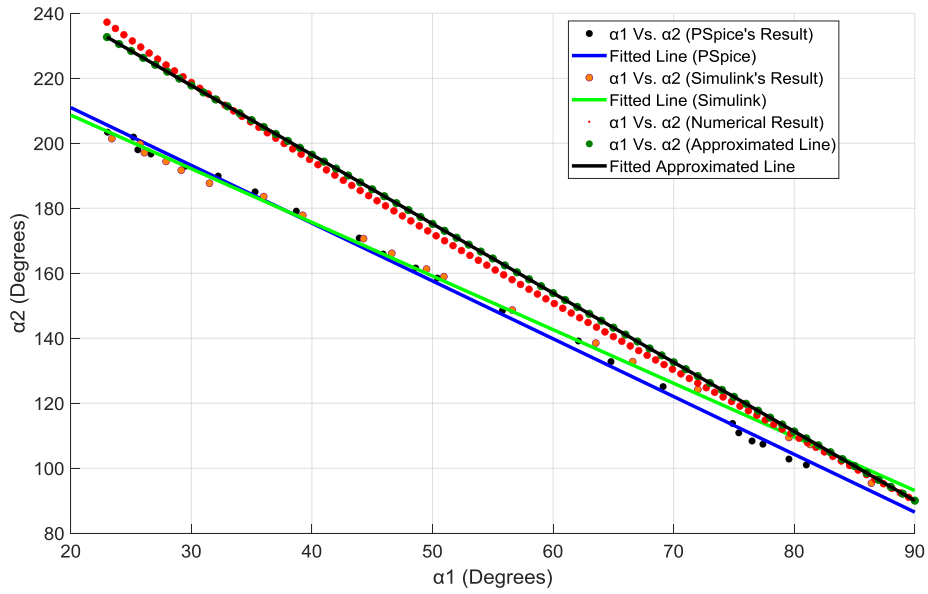


**Figure 3.19.**  $\alpha_1$  vs.  $\alpha_2$  from simulation results and numerical results.

The mean percentage error between the numerical and Simulink results was found to be 7.22% and it was 8.64% between the numerical and the PSpice results.

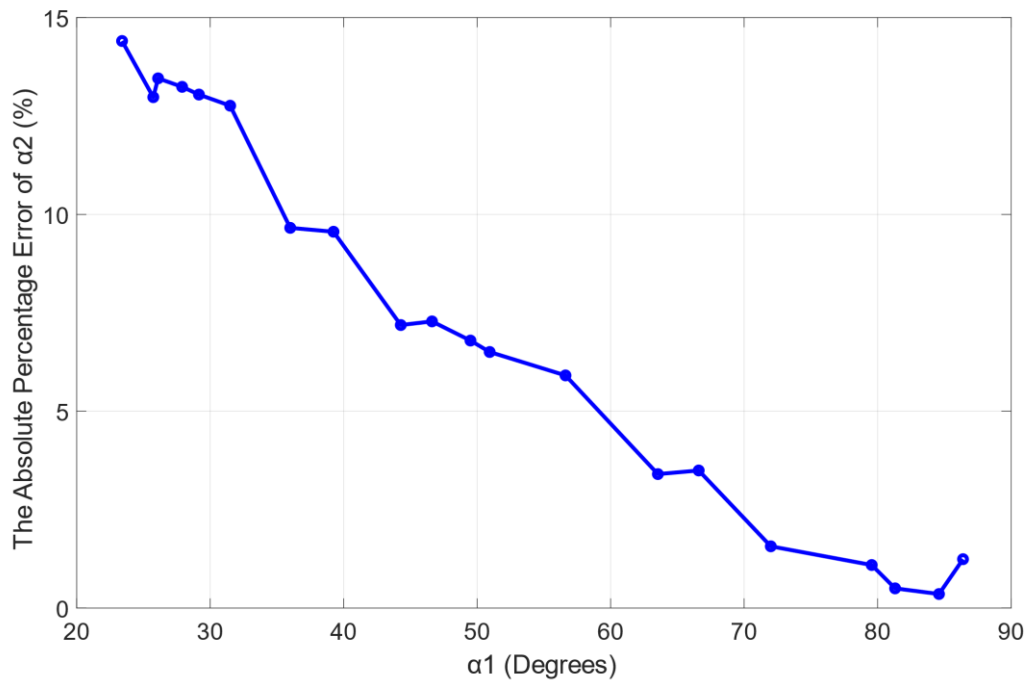


**Figure 3.20.** The absolute percentage error of  $\alpha_2$  values between the numerical result and the Simulink simulation result as a function of  $\alpha_1$ .

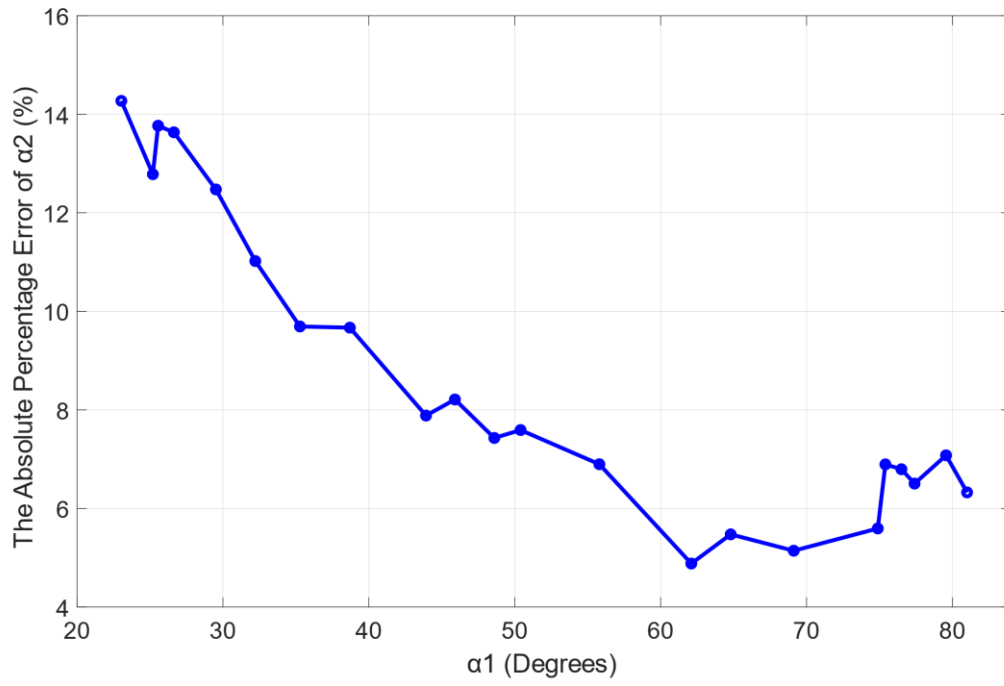


**Figure 3.21.** The absolute percentage error of  $\alpha_2$  values between the numerical result and the PSpice simulation result as a function of  $\alpha_1$ .

## 4. THE EXPERIMENTAL RESULTS

The experimental system consists of the autotransformer, the isolation step-down transformer, the rectifier circuit, the oscilloscope, the measurement probes and the personal computer. Figure 4.1 shows the block diagram of the entire system used in the experiment.

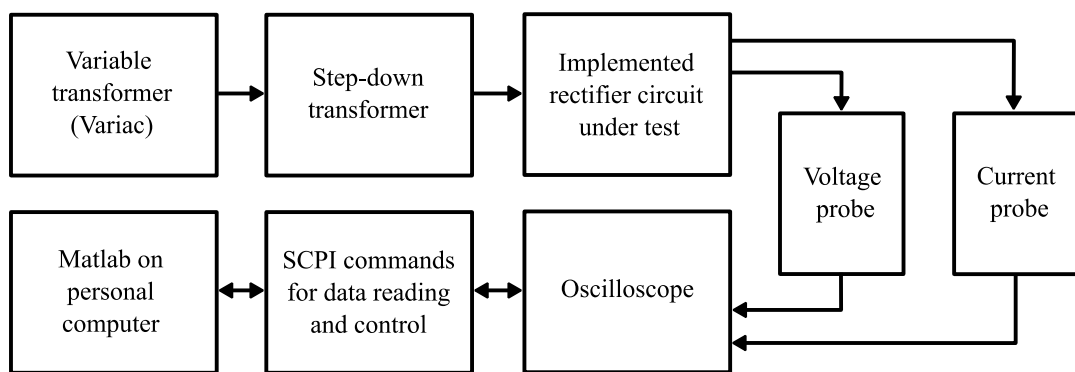


**Figure 4.1.** Block diagram of the complete experimental system.

### 4.1. Elements of the Implemented Rectifier System

#### 4.1.1. The autotransformer (variac)

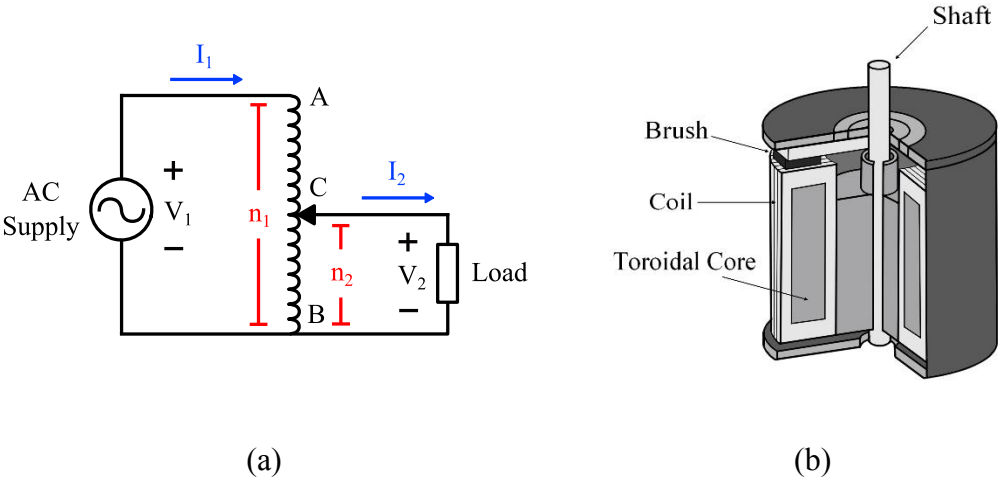
The autotransformer (variac) offers the ability to adjust its AC output voltage amplitude to a certain desired value, it is especially important for this research because a wide range of the rectifier's input voltage amplitudes was required to deliver the circuit with enough resulting range of input current amplitudes, to check how the experimental circuit results follow the theory. The autotransformer consists of a single winding, which is considered as the primary and secondary winding at the same time, contrary to the conventional transformer that has two windings, the single winding of an autotransformer results in the output and input of the transformer being electrically connected, which means that it lacks the isolation feature and it is magnetically connected by self-induction.

Figure 4.2 (a) shows the diagram of a standard step-down autotransformer, where three terminals on the single winding can be noticed, A, B and C. The complete number of

turns of the primary winding ( $n_1$ ) is located between the two terminals A and B, whereas the turns' number between C and B ( $n_2$ ) represents the secondary winding, the variac's output voltage can be calculated as in equation 4.1 [37]:

$$V_2 = V_1(n_2/n_1) \tag{4.1}$$

The typical construction of a manufactured variac is shown in figure 4.2 (b), it includes a brush that has a rotating mechanism throughout the entire winding, therefore, it provides fine control over the output voltage value by the position in which it's placed, the supported output voltage range that variacs can usually supply is from 0% to a little higher than 100% of the input voltage. Variacs can be operated manually or have motors that perform the automatic rotation as a part of the automated voltage regulation functionality. The copper winding is used on a toroidal core, that core shape prevents high levels of noise due to having a low electromagnetic dispersion. Carbon is usually used to make the brush, variacs are highly efficient devices, with about a 98% efficiency rate [38].



**Figure 4.2.** (a) The schematic of a standard step-down autotransformer, and (b) The construction of a typical autotransformer.

The experimentally used autotransformer has a 1 KVA rating at its maximum operation, it has a single-phase input for the mains electricity of 220 V, three-terminal output, one being the earth connected, which was neglected in the experiment and the two remaining terminals were used to feed the following step-down isolation transformer. The variac doesn't offer an earth isolation functionality.

The variac offers a manual adjusting mechanism over the output voltage, the handy knob can be rotated across the complete range of the output marks, starting from 0% which is proportional to 0 V output, up until 100% which is proportional to 220 V output. Adjusting the knob works by changing the placement of the brush in accordance with the winding of the transformer, resulting in a change in the output voltage. To ensure a robust connection between the variac and the isolation transformer, which comes after the variac, a cable with banana connectors at the variac output terminals side was used. Figure 4.3 shows an image of the utilized autotransformer.



**Figure 4.3.** The experimentally used autotransformer (variac).

#### **4.1.2. The isolation transformer**

Despite that the variac offers control over the output voltage amplitude, using the variac's knob to adjust the voltage level to a value lower than the maximum output voltage of the variac (220 V) can lack precision, so more precise adjustment can be achieved using an additional (typical) step-down transformer that has a narrower conversion ratio of 18.33:1.

The utilized unit is a centre-tapped transformer, it has two output voltage options, 24 V and 12 V output terminals, The 12 V output terminal was neglected. The second terminal is rated to supply 24 V of maximum RMS voltage, where the transformer

transforms the utility's 220 V into rated 24 V RMS voltage, which is the equivalent of about 33.94 V peak voltage and that maximum peak was enough for the practical experiment.

The transformer offers an isolation feature, which is beneficial since the variac is earthed and the used oscilloscope is also earthed, so the short-circuit problem was avoided by the transformer's isolation feature. The isolation transformer is rated at a maximum output power of 100 VA.

#### **4.1.3. The AC side smoothing inductor**

The implemented rectifier circuit utilizes a current smoothing inductor at the input side, that inductor smooths the source current and its characteristics are essential for the analysis part of this research. The practical experiments were initially done with various types of inductors. The experiments showed that an inductor with a high current tolerance rating is required to work properly with the circuit. When a typical inductor rated at 1 A or lower was used with the circuit and in the case of having higher current amplitudes flowing through that inductor, there was high-temperature heat-radiation from the inductor, and even dissolving of the outer isolating material covering the inductor in some cases.

The inductor which have been used in this research is rated to handle up to 4 A, RMS current, and it has a 330 $\mu$ H of inductance value. Inductors with a higher inductance rating were also tested with the rectifier circuit, the problem is with higher inductance comes higher inductive reactance  $X_L$ , which causes a reduction in the amplitude of the flowing current, and that goes against the desired measurement needs of having higher current amplitudes to calculate as much as possible more values for the conduction angles. Figure 4.4 shows the three inductor models tested with the rectifier circuit.



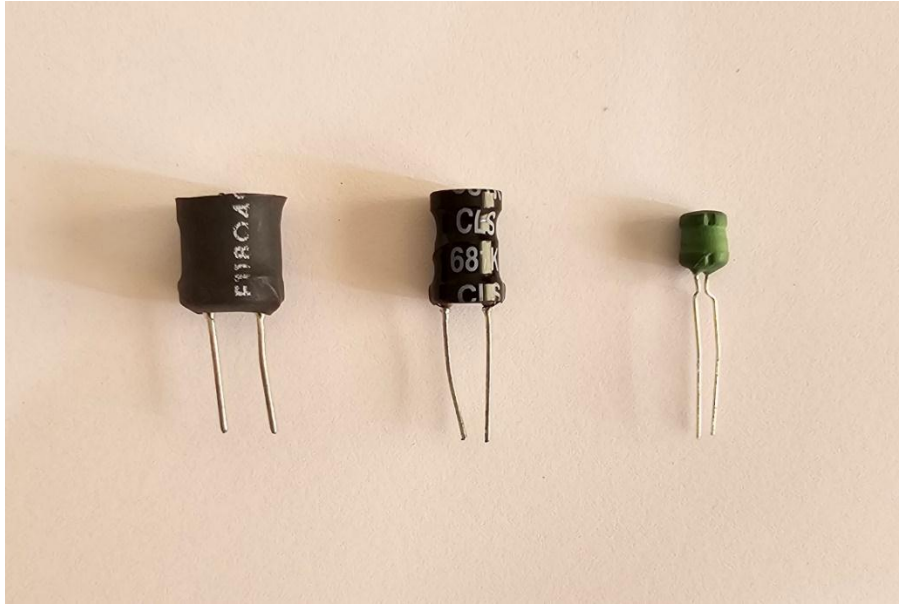


**Figure 4.4.** The three inductor models that have been tested with the circuit.

#### **4.1.4. The single-phase bridge rectifier**

Since there was high current flow through the rectifier circuit, a diode model with the proper specifications was needed to endure that current and for that purpose, Schottky diodes were the proper choice. Schottky diodes don't only offer high current tolerance, but they also have a low forward voltage rating, making them very suitable for applications where a low voltage drop is required with an electrical circuit application and they support high-frequency operation [39].

In the implementation of the rectifier circuit, the MBR560 model Schottky diode was used, it has 5 A of RMS current tolerance and a 0.4 V of forward voltage rating [39]. When 7.95 A of peak current amplitude was reached during the experimental circuit operation, the diode kept being fully functional without a problem.

Figure 4.5 shows the full-wave bridge-rectifier circuit built using four MBR560 model Schottky diodes, the rectifier's diodes were soldered on a prototype PCB to ensure a strong connection among them, with the cables at the terminals connected to the circuit's input and output.

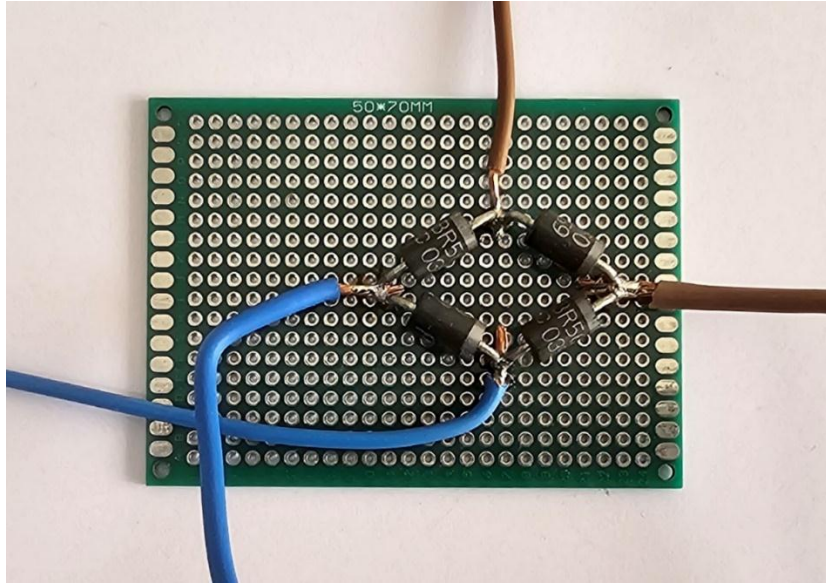


**Figure 4.5.** The implemented rectifier circuit was made using MBR560 Schottky diodes.

#### **4.1.5. Lead-acid battery as a constant voltage load**

One of the main aspects of this study is to use a constant voltage load, and for the experimental work, two batteries were used, the first with a 12 V, 12 Ah rating, and the second with 12 V, 9 Ah rating, both of them are sealed lead-acid batteries shown in figure 4.6, and they have been used as the load with constant DC output voltage.



**Figure 4.6.** The lead acid batteries that have been used in the experiment.

## **4.2. The Measurement System**

The main device in the measurement system is the oscilloscope, it is where the essential reading and process of data happens, then transferred to the personal computer for plotting. The electrical readings regarding voltage and current are carried out to the oscilloscope using the voltage probe and current probe.

### **4.2.1. SCPI instrument control language**

SCPI stands for (Standard Commands for Programmable Instrumentation), it is an instrument control language that is based on IEEE 488.2 standard. This language enables the remote controllability of instruments such as DC power supplies, spectrum analyzers, function generators, oscilloscopes, and other instruments that support this language, without direct and physical contact with the device itself [40].

The structure of the language's syntax includes a section-based developing approach, where the command starts with a keyword at the beginning, and then sub-words could come to direct more specific commands. Despite that the command sets of commercial instruments might be different, or even have some differences among models produced by the same manufacturer, an SCPI command can either be set or query command. Set commands are beneficial to set the acquiring mode for example, or change any desired feature while acquiring measurements, while a query command gives back feedback from the instrument about certain characteristics that the device was asked about, like signal amplitudes or sampling rate or even to acquire the signal's sampled data to plot the waveform on the personal computer [41], [42].

The major feature that SCPI language supports, and this research made use of, is the ability to include SCPI commands inside a high-level language like MATLAB, LabVIEW, or C/C++ [42]. The integration between SCPI and another programming environment provides greater potential for developing complex algorithms that perform dynamic operations, this research is an example, where SCPI commands were integrated with MATLAB syntax to perform several steps required to acquire the voltage and current signals with the required quality and accuracy. The connection was carried out using a USB cable, utilizing the USB serial port on both the computer and the oscilloscope.

The SCPI language offered a successful alternative to the inconvenient manual control which wouldn't suit the needs of this study properly.

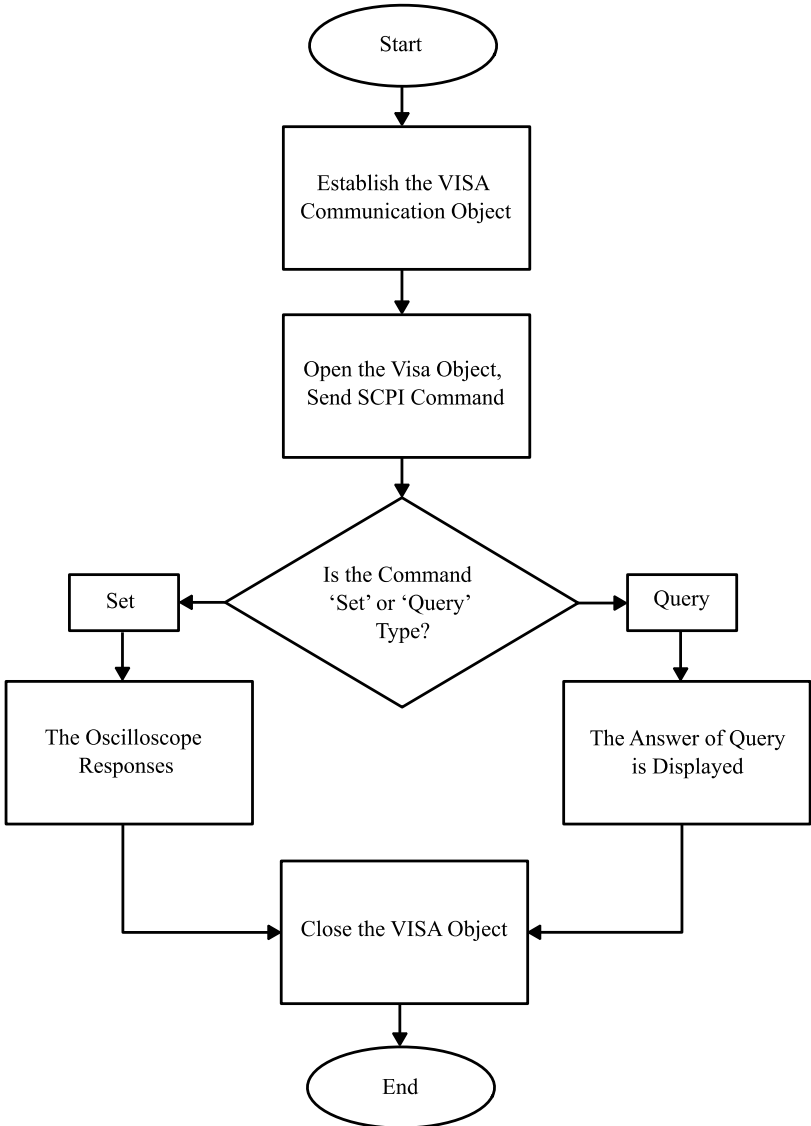


**Figure 4.7.** The basic communication algorithm between the computer and the oscilloscope using SCPI commands.

**4.2.2. The oscilloscope**

The oscilloscope is an end-user-oriented measurement device that performs several operations and has a wide set of features that are useful for signal reading and processing, where it utilizes an analogue to digital converter (ADC) with 1 Giga Sample per second sampling rate, shared among all channels. The ADC is an essential component to enable the function of sampling the analogue signal and converting it into a digital signal [43]. Besides that, the oscilloscope has different signal-acquiring modes and it's a storage device, that offers the ability to precisely examine the acquired

signal using scaling features, it performs measurements correctly, some models have high resolution, and finally, it can be controlled remotely which is a feature that was invested in this research.

The oscilloscope model used in this research is Rigol DS1054Z which has four analogue channels, two of which were used in the experiments, and it has a 50 MHz bandwidth, 24 mega point of memory depth, and an 8-bit analogue to digital converter. The oscilloscope can be remotely controlled using SCPI language and also to exchange data between it and a supported software on the computer, which happens through either the USB serial port or LAN port, available at the back side of the device.

The USB serial port was chosen for connection with the personal computer for controlling the instrument and for data acquisition. The instrument's necessary drivers provided by the manufacturer were installed on the computer to avoid any problems in connection between them.

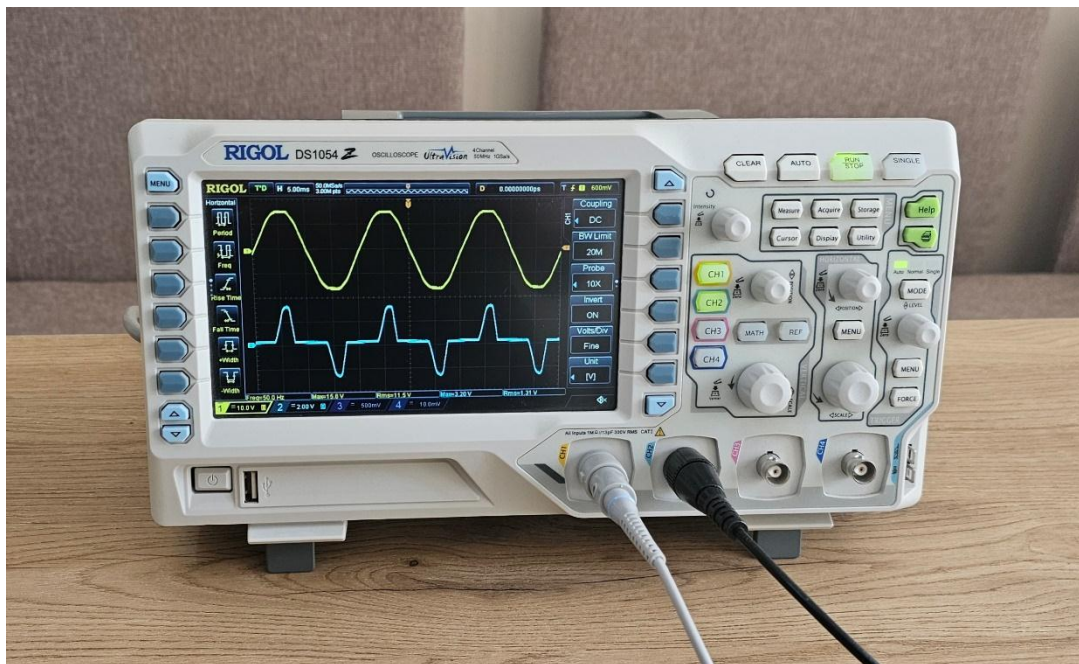


**Figure 4.8.** The oscilloscope model used for electrical measurements of the circuit.

### 4.2.3. The current measurement probe

A current probe was used to carry out the current measurements. The chosen device transforms the electrical current being measured into a voltage; because an oscilloscope can only read voltage signals, that voltage value detected by the oscilloscope is directly proportional to the measured current value and waveform, and for that purpose, a current probe that utilizes a Hall effect sensor was used.

The Hall effect sensor's working principle can be explained as if there is a thin layer of semiconductor that is connected to a constant voltage source (DC), there will be a steady current flow through it, and when having a magnetic field placed in a perpendicular orientation to this semiconductor, there will be a reaction between the magnetic field of the mentioned current and the magnetic field of the outsource, that will push the electrons to flow across the semiconductor reaching one side of it, creating a potential difference, which is called Hall voltage, that voltage increases proportionally with the strength increment of the magnetic field, as shown in figure 4.9.

The force that moves the electrons towards the sides is called Lorentz force, which can be defined as the force that impacts the particles by the effect of electrical and magnetic fields. The Hall effect can be introduced in sensor form, as a method to measure the magnetic field strength, and other applications including position, pressure, and current sensing [44], [45].

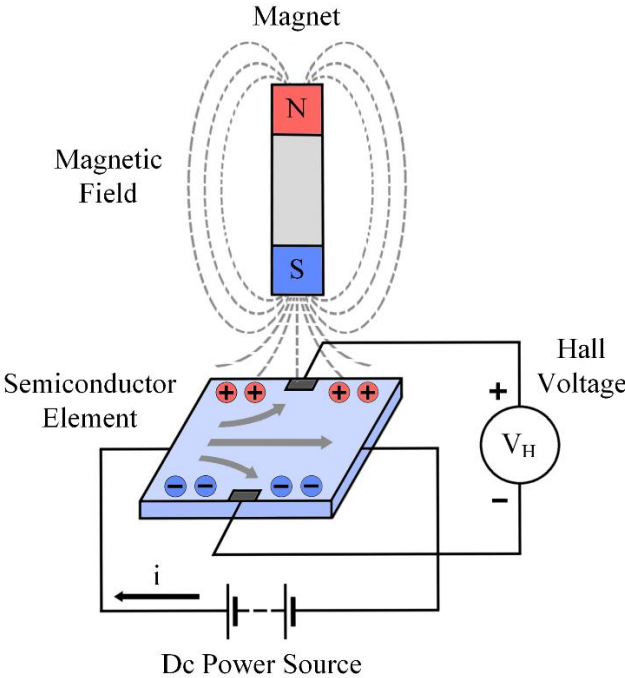


**Figure 4.9.** The working principle of the Hall effect sensor.

The current probe which have been used is a Hantek CC-65 AC/DC current clamp, it utilizes a Hall effect sensor to detect the current's magnetic field. The device has several beneficial features for the experimental work of this thesis. First, the clamp-type jaws of the probe, they offer the ability to use the device without the need to break



the circuit under test, and when the jaw of the clamp closes, it offers a rather small gap around the wire, which improves the reading accuracy.

The device has a sliding switch that offers the ability to choose among closing it off, a 1mV/10mA or 1mV/100mA attenuation levels. The 1mV/100mA option can be chosen when measuring more than 2 A of electrical current. The probe can measure up to 65 A and supports up to 20 KHz of operational frequency. During the use of the probe, an in-body provided degaussing button should be pressed regularly to decrease or zero the remnant magnetic field, where the reading level of the waveform should appear at the zero level on the oscilloscope screen, to acquire an accurate current reading [46]. The current probe is shown in figure 4.10.



**Figure 4.10.** The practically used current measurement probe.

### **4.3. Acquiring the Experimental System's Electrical Measurements**

The entire experimental system consisted of the rectifier circuit and the measurement system is called the experimental system. The results acquired from this system represent how the implemented circuit performs. The combination of compatible system elements and the data-adjustment algorithms made getting the experimental electrical measurements and sending them automatically to MATLAB for plotting convenient and easy, besides offering accurate results.

### 4.3.1. Operating the experimental system

The complete experimental system is shown in figure 4.11, to configure the correct amplitude of the AC input voltage for the circuit, the operation starts with the variac, which is connected to the step-down isolation transformer. The variac's rotatable adjustment knob provides control over the voltage amplitude easily, there are times during experiments when the mains electricity is not stable, so the variac not only gives the desired voltage amplitude but also offers a fast and easy adjustment method for utility voltage's unstable supply situations.

The physical parts of the process of preparing the complete experimental system for executing the experiments include connecting the variac to the mains electricity and then connecting the isolation transformer to it, the output of the transformer is then connected to the rectifier circuit using quick-connect terminals, this type of connectors is also used with the battery's terminals.

The voltage probe can be attached to the input or output side of the circuit, depending on which voltage is desired to be measured, the current probe follows that with its clamping mechanism. Other things may include connecting the USB cable between the oscilloscope and the personal computer and connecting the oscilloscope itself to electricity.

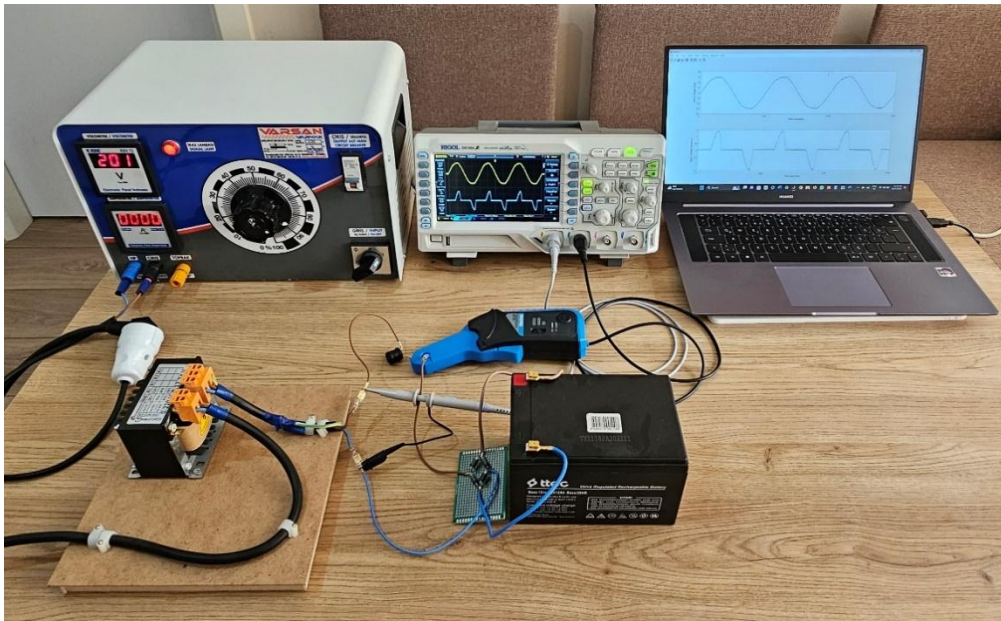


**Figure 4.11.** The complete experimental system.



### **4.3.2. The autonomous measurement and data processing algorithm**

The autonomous algorithm includes executing the tasks of remote control of the oscilloscope, acquiring the measurement data and plotting them properly. To acquire the signal's properties, the oscilloscope can use separated functions to detect, for example, the peak amplitude of the voltage being measured, which is called the maximum voltage (VMAX), besides other functions, like minimum voltage or RMS voltage, etc, and it is possible to activate these functions with physical buttons or using SCPI commands dedicated for them, so that MATLAB on the personal computer will detect the characteristics of the voltage being measured and adjust the fetched data accordingly.

A series of SCPI commands associated with this operation is required to plot the signals accurately in MATLAB, these SCPI commands are a combination of query and set commands. First, the correct source channel of the wave is selected, then, the data consisting of samples of the analogue signal is acquired, then the oscilloscope will be asked about the detected maximum voltage amplitude. After that, MATLAB will correctly scale the received data of the wave to the detected maximum voltage according to the oscilloscope's feedback.

Calculating the input current's two conduction angles,  $\alpha_1$ , and  $\alpha_2$ , using the waveform acquired from the experimental system involves a multi-stage processing which is part of the automated algorithm. When configuring the input voltage amplitude using the variac's adjustment knob, the vertical scale of the rectifier system's input voltage and input current, on the oscilloscope's screen, will be changed, which can cause faults and effects the angles' detection accuracy.

To achieve a convenient approach to calculating the angles accurately across the range of the tested amplitudes of the electrical current, the vertical scaling of the input current being displayed on the oscilloscope should always be kept constant through all the tested cases. That was achieved by connecting the adjustment of the amplitude divisions with the current's peak readings, by that, if the current amplitude would increase or decrease, and that would be displayed on the oscilloscope's display, the algorithm will always scale it correctly to constant vertical divisions.

The algorithm makes the correct horizontal alignment to the acquired input voltage, to ensure one complete cycle of the voltage is presented, which will make the input

current waveform correctly aligned too, this is important for correct time and conduction angles' calculation. The conduction angles are calculated at a 5% height level of the positive half period of the input current waveform for each test case, where the algorithm will detect the first 5% of the input current's rising edge and calculate the time at which the conduction occurred, then calculate the turn on angle in degrees, then it will detect the last 5% of the falling edge of that waveform, and calculate the corresponding time and the turn off angle. The reason behind choosing the 5% threshold for the angle detection from the input current's waveform is that the current waveform in the experiment is not ideal, and the presented oscillations in the current waveform can confuse the algorithm, especially for angle detection in lower current amplitudes.

By the previous explanation, it appears how crucial the SCPI control language is in this study, because besides providing the data transfer functionality to the personal computer, it enables the necessary controllability of the oscilloscope to scale the waveforms of the input voltage and input current to constant division scales to achieve correct conduction angles' detection across all the ranges that were tested, which offered a superior alternative to the manual adjustments that could have been needed to be made on the oscilloscope using physical buttons and knobs. For each testing case, which can result in an inconsistent detection of the conduction angles due to the fault margin caused by the manual operation, therefore, an automated algorithm utilizing the SCPI language was developed, used, and proved successful.

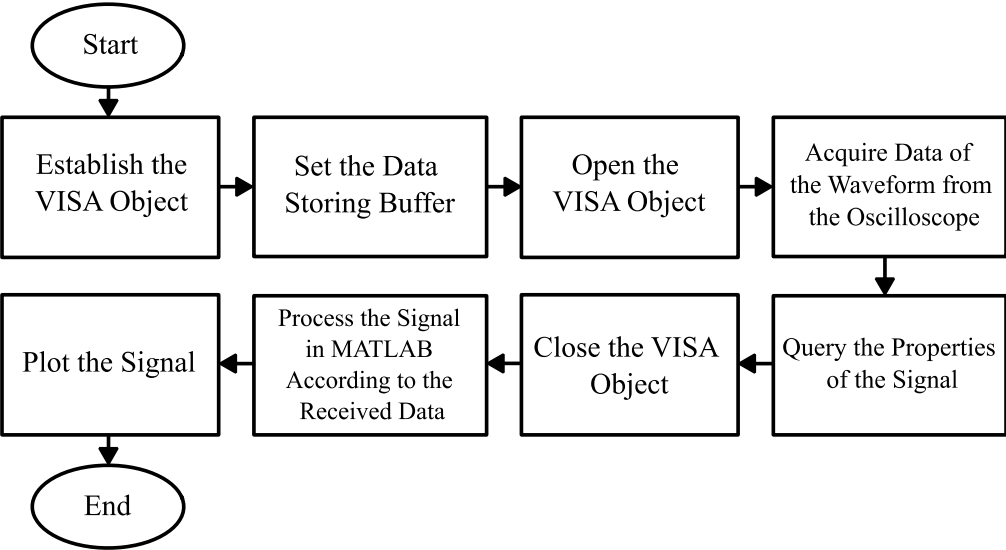


**Figure 4.12.** The waveform data and signal properties acquiring algorithm.

### 4.3.3. Measurement results of the experimental system

Two channels of the oscilloscope were used in each measurement experiment, which is sufficient for obtaining both the input and output main characteristics, where the input voltage and input current were acquired at one time and the measurement probes were moved to the output side of the implemented circuit for the output voltage and output current acquiring in the second case. The oscilloscope provides 1200 points as an array's values in MATLAB, these values represent the sampled amplitudes of the analogue signal.

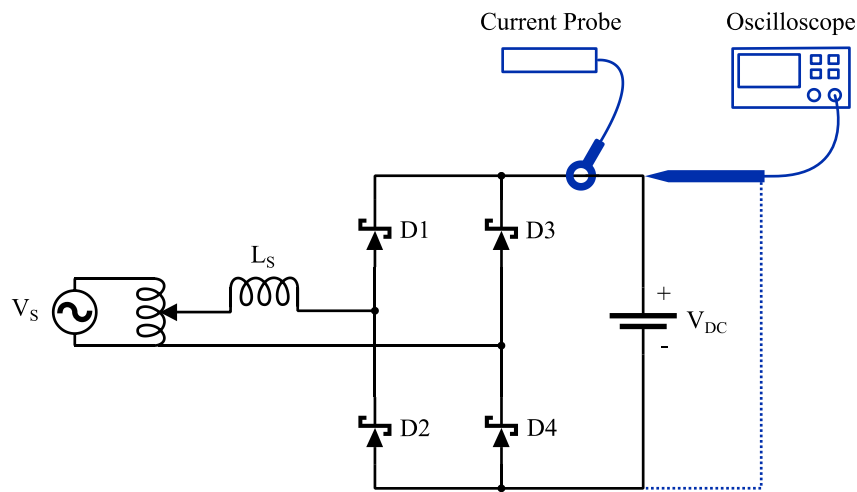


**Figure 4.13.** Schematic of the implemented rectifier circuit with the measurement probes being connected.

The first measurements were made with the rectifier circuit connected to a 12 V, 12 Ah battery, the utility voltage was used in the experiments, the input voltage amplitude was reduced utilizing the variac and the step-down isolation transformer and the input voltage and input current obtained from the experimental system are given in figure 4.14 (a) and figure 4.14 (b). It can be noticed that the utility voltage is very near to the sinusoidal waveform given in the simulations, but it is not a pure sinusoidal wave, the input current also shows a very close behaviour to the simulations results, where it has pluses that look like triangles in each half cycle, and working in discontinuous conduction mode. The turn on and turn off angles of the rectifier are affected by the forward voltage of the diodes, the utility voltage not being a pure sine wave, and the output's voltage values.

The utility’s voltage amplitude was reduced to 16 V, the constant DC output voltage amplitude was 13.3 V with 100 mV of voltage ripple, and the current’s amplitude was 2.48 A.

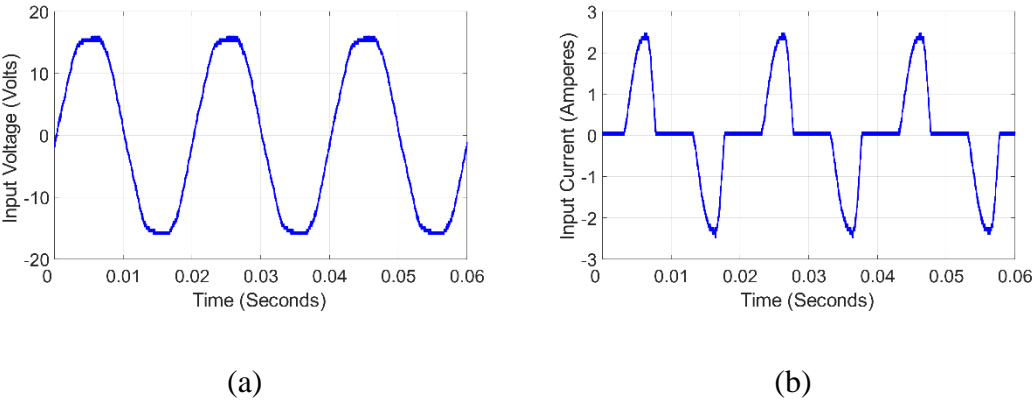


**Figure 4.14.** The experimental circuit’s measurements made with the 12 Ah battery load, for (a) Input voltage, and (b) Input current.

All practical lead acid batteries possess an inherent internal resistance, regardless of its magnitude. As a result of this resistance, when the rectifier is in operation, the pulsative nature of the flowing current will induce a pulsating ripple in the output voltage. The output voltage, denoted as  $V_{out}$ , can be expressed using the equation  $V_{out} = i_{rec}(t)R_{battery} + V_{dc}$ , where  $R_{battery}$  represents the battery’s internal resistance [47].

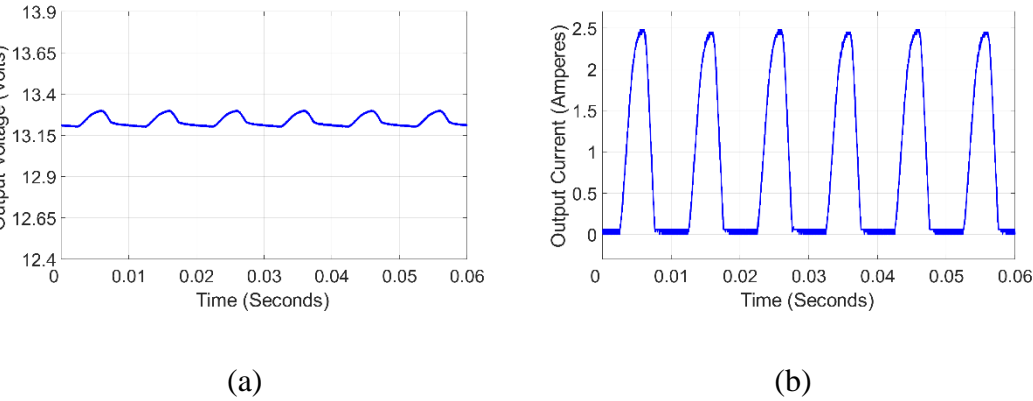


**Figure 4.15.** The experimental circuit’s measurements made with the 12 Ah battery load, for (a) Output voltage, and (b) Output current.

The measurements with another battery as the constant load were made to examine if there would be any big difference between the electrical measurements obtained with either of the two batteries regarding the waveform and the wave amplitude, the second battery has also a 12 V nominal voltage rating, it is a lead acid battery, but with 9 Ah

rating, after taking the measurements with it being the load, very similar electrical measurements were obtained compared to using the 12 Ah battery as the constant load, that similarity was regarding the waveforms and the wave's amplitudes.

The rectifier was supplied with 16.4 V of input voltage amplitude, the DC output voltage amplitude was 13.6 V, with about 100 mV of ripple, and the current amplitude was 2.42 A. The measurement results regarding this test case are given in figure 4.16 and figure 4.17.

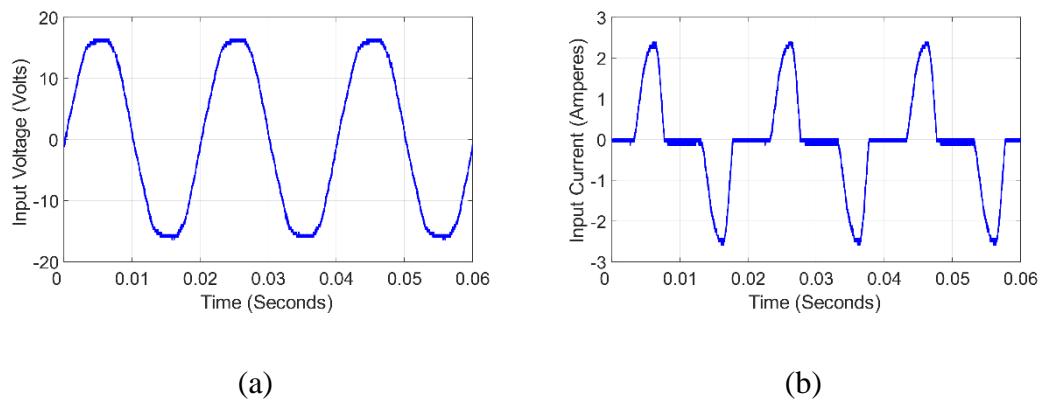


**Figure 4.16.** The experimental circuit's measurements made with the 9 Ah battery load, for (a) Input voltage, and (b) Input current.

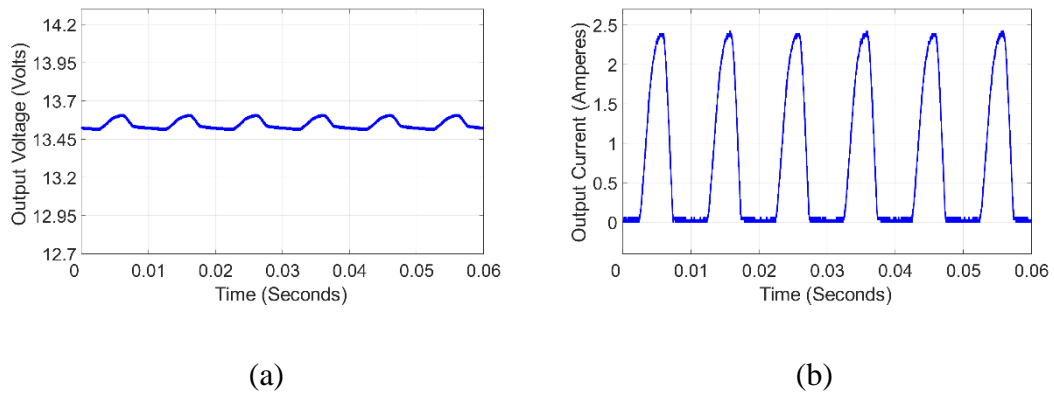


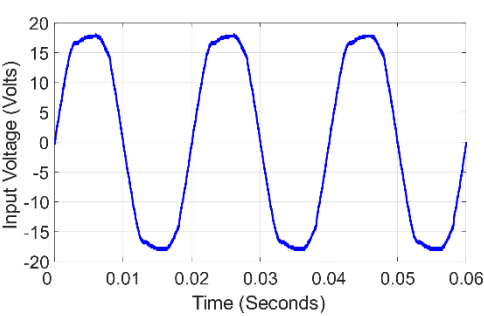
**Figure 4.17.** The experimental circuit's measurements made with the 9 Ah battery load, for (a) Output voltage, and (b) Output current.

#### 4.3.4. A higher current measurement case

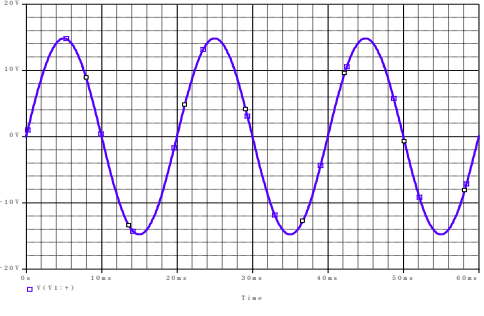
Another test case was performed, but with a higher current amplitude, and the measurements of the experimental system are given side by side with the PSpice's simulation results. While using the 12 Ah battery as the load, the implemented rectifier circuit was supplied with 18.09 V of input voltage amplitude, which made the DC

output voltage on the battery's terminals reach 13.5 V. That potential difference allowed 5 A of current amplitude to flow through the circuit. For the PSpice's parameters, the input voltage needed to be adjusted to 14.8 V, and the DC voltage was kept at 12.75 V, which allowed a 4.99 A of current amplitude to be achieved.

It can be noticed that the discontinuous conduction mode was conserved and the waveforms of the simulation and experiment are close to each other, besides the constant DC output voltage, where the DC output voltage of the practical system showed about 260 mV of voltage ripple and the PSpice's result showed about 5 mV of voltage ripple.

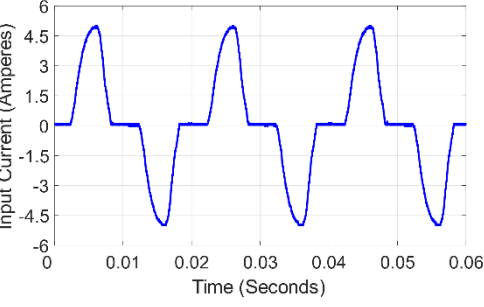


(a)

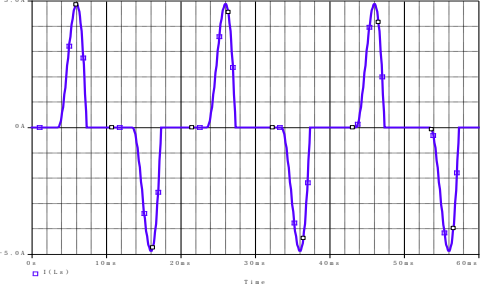


(b)

**Figure 4.18.** Input voltage waveform for (a) The experimental rectifier circuit, and (b) PSpice.

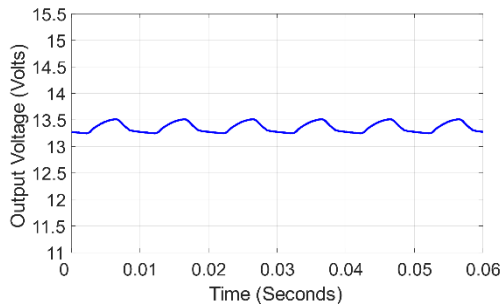


(a)

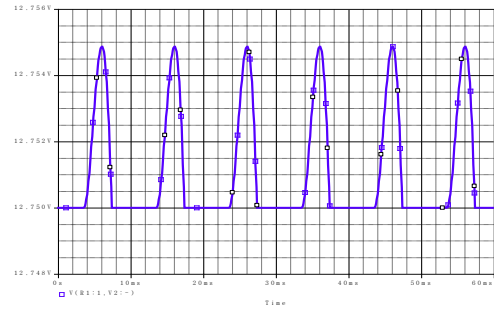


(b)

**Figure 4.19.** Input current waveform for (a) The experimental rectifier circuit, and (b) PSpice.

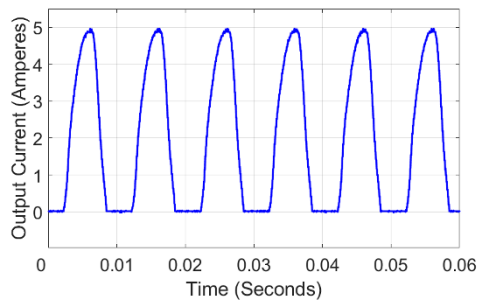


(a)

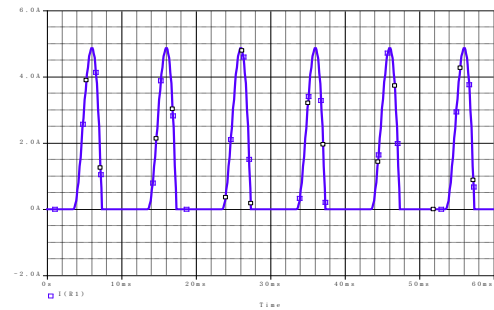


(b)

**Figure 4.20.** Output voltage waveform for (a) The experimental rectifier circuit, and (b) PSpice.



(a)



(b)

**Figure 4.21.** Output current waveform for (a) The experimental rectifier circuit, and (b) PSpice.

#### 4.4. The Relation Between the Conduction Angles

Plotting the relation between the conduction angles ( $\alpha_1$  and  $\alpha_2$ ) of the experimental system requires supplying the rectifier circuit with multiple values of input voltage, to have different potential differences between the input voltage and output load voltage, which will result in a varying input current amplitudes to flow through the circuit, hence, various values for conduction angles.

When the 12 Ah battery was used as a load, the variac was adjusted to supply the rectifier circuit with the input voltage amplitude in the range of 13.65 V to 20.22 V, which made the DC output voltage on the battery's terminal range between 12.51 V to 13.5 V. This range of potential difference allowed the electrical current to flow through the circuit with a range between 0 A to 7.95 A, as peak current values. A maximum of

23 values were calculated for the  $\alpha_1$  and  $\alpha_2$ , where  $\alpha_1$  values were located between  $39.8^\circ$  to  $84.2^\circ$ .

To consider the voltage drop on the Schottky diodes and its effect on conduction angles' calculation for the theoretical part, 0.4 V was added for each of the two series diodes that work at each half cycle to the turn on angle ( $\alpha_1$ ) calculation formula, as given in equation 4.2.

$$\alpha_1 = \arcsin ( V_{dc} / V_m - 2V_{diode} ) \quad (4.2)$$

To find the corresponding  $\alpha_2$  value, the previous formula that describes  $\alpha_1$  and  $\alpha_2$  relation can be recalled:

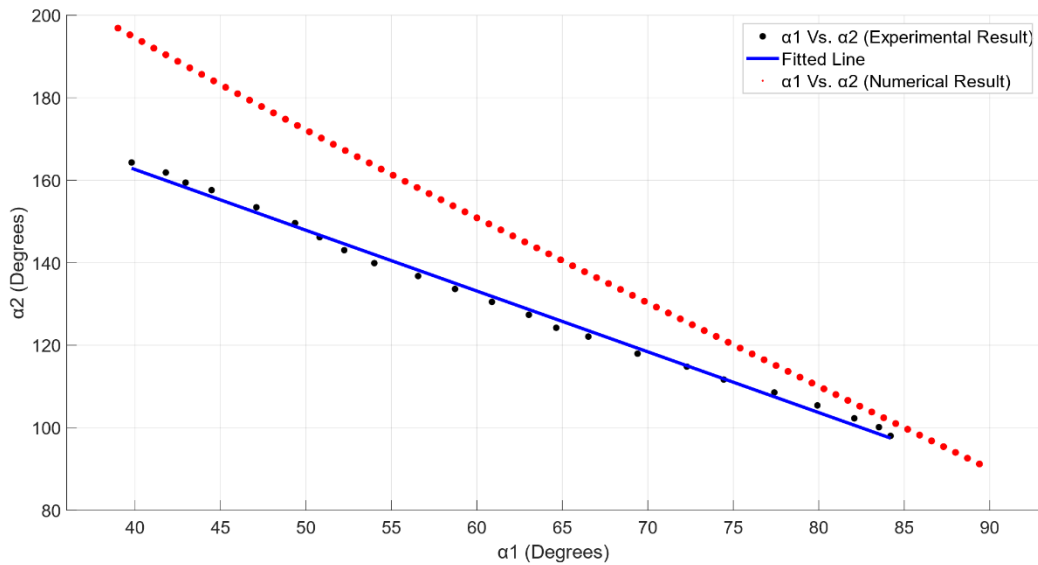
$$f(\alpha_2) = \cos \alpha_1 - \cos \alpha_2 + \sin \alpha_1 (\alpha_1 - \alpha_2) = 0 \quad (4.3)$$

Figure 4.22 shows the relation between  $\alpha_1$  and  $\alpha_2$  calculated from both the experiment and the theory when the 12 Ah battery load was used. Figure 4.23 shows their relation when the 9 Ah battery was used.

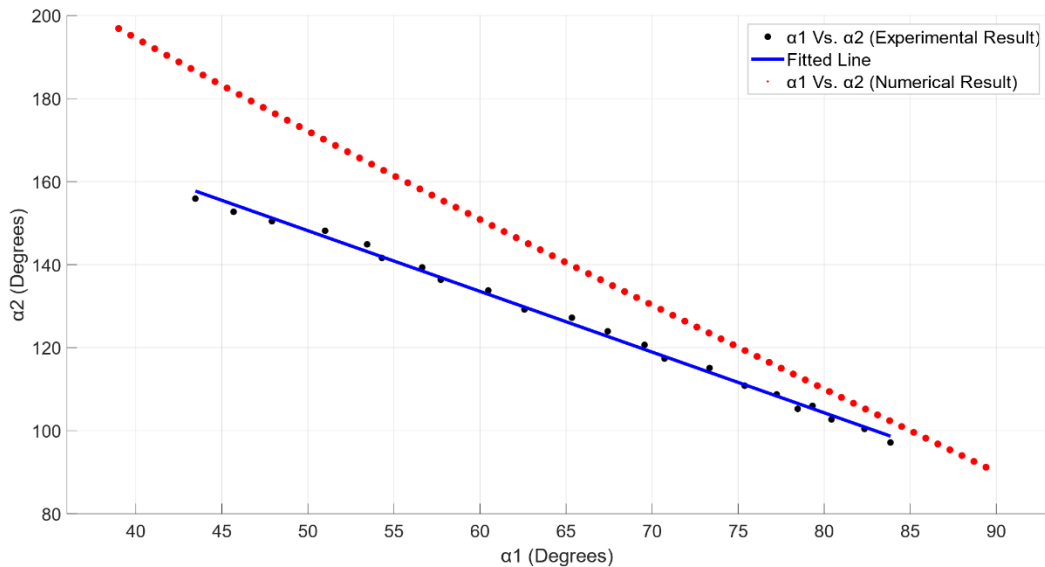
To present the complete results more comprehensively, figure 4.24 and figure 4.25 include the line regression of the numerical result, the approximated line, the two simulation software results, and the experimental results altogether.

The major thing that can be observed from these two figures is the relation between the conduction angles obtained from the experimental work is still almost linear, which shows a similar relation obtained from the numerical solution and also the simulation result given in the third chapter. The slope of the line is different when the numerical, simulation, and experimental results are compared, that difference is believed to be present as a result of the utility voltage's distortion, the diodes' forward voltage, the output voltage's pulsed nature, and the battery's internal resistance.



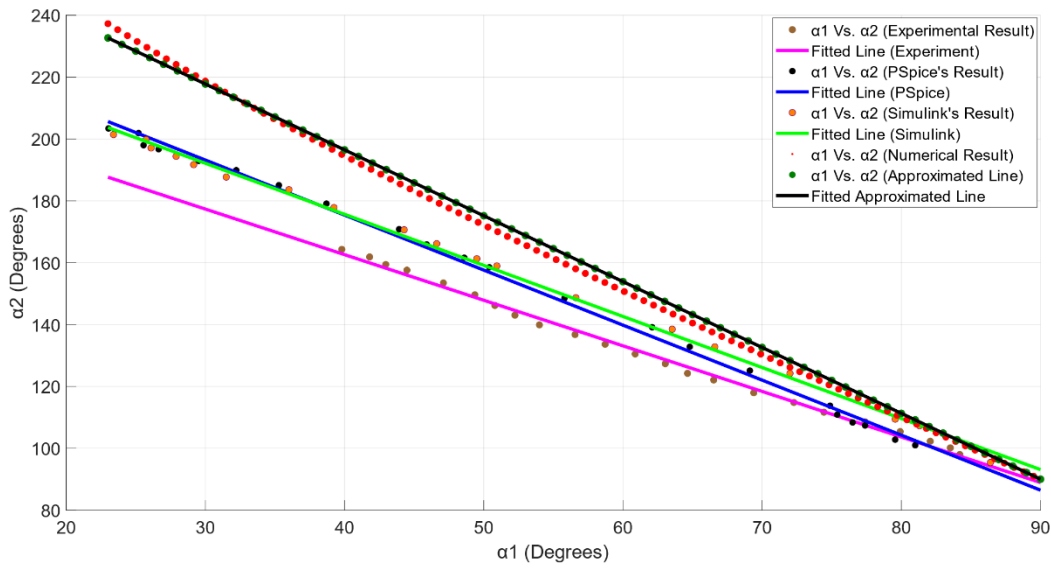


**Figure 4.22.** The relation between  $\alpha_1$  and  $\alpha_2$  calculated from both the numerical solution and the experiment when the 12 Ah battery was used.

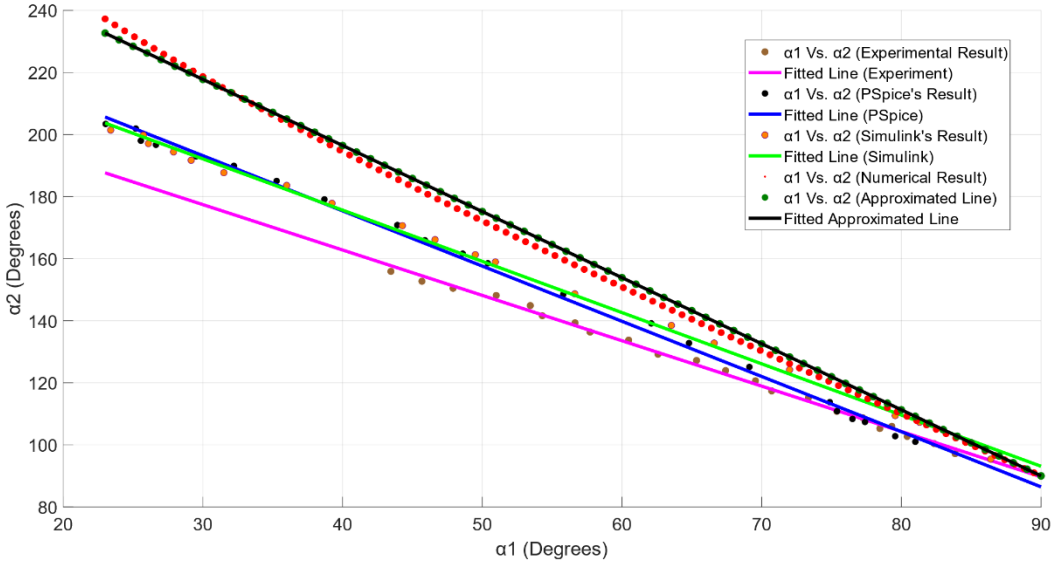


**Figure 4.23.** The relation between  $\alpha_1$  and  $\alpha_2$  calculated from both the numerical solution and the experiment when the 9 Ah battery was used.

It was found that the 12 Ah battery draws more current compared to the 9 Ah battery when they were supplied with the same DC voltage amplitude, and even if the batteries do not withdraw significantly different current amplitudes, it was useful to have the higher current reading with the 12 Ah battery because it allowed for additional values of the conduction angles to be calculated. As for the relation between the conduction angles obtained from the two batteries, they were very close to each other, where the line slopes were not that different between the two batteries' results.

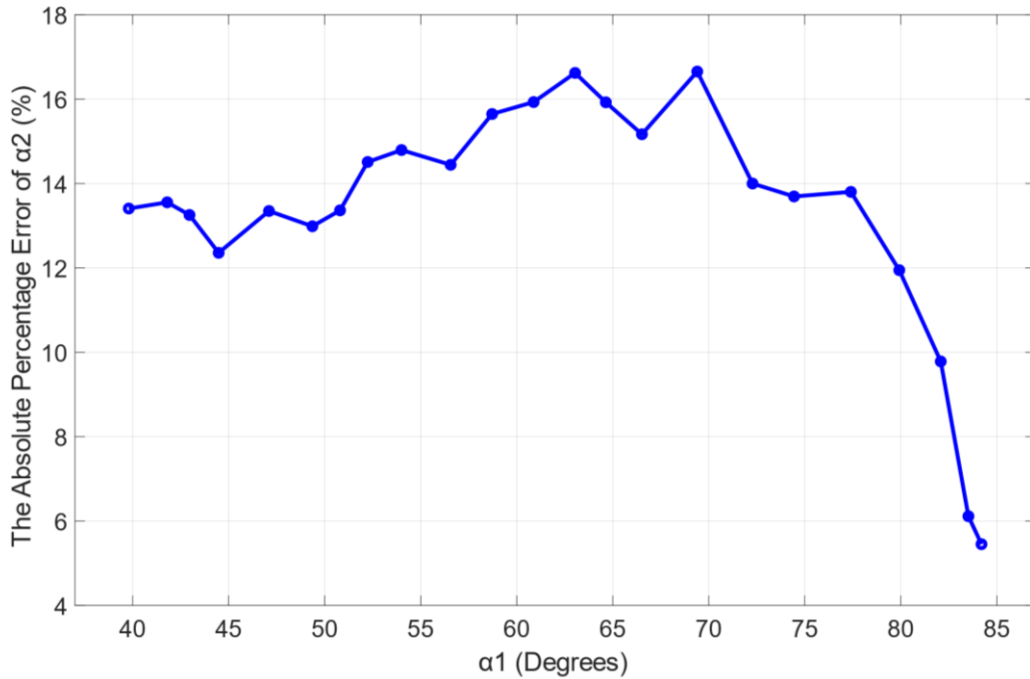


**Figure 4.24.** The calculated results from the numerical solution, the approximated line, the simulation, and the experiment with the 12 Ah battery.



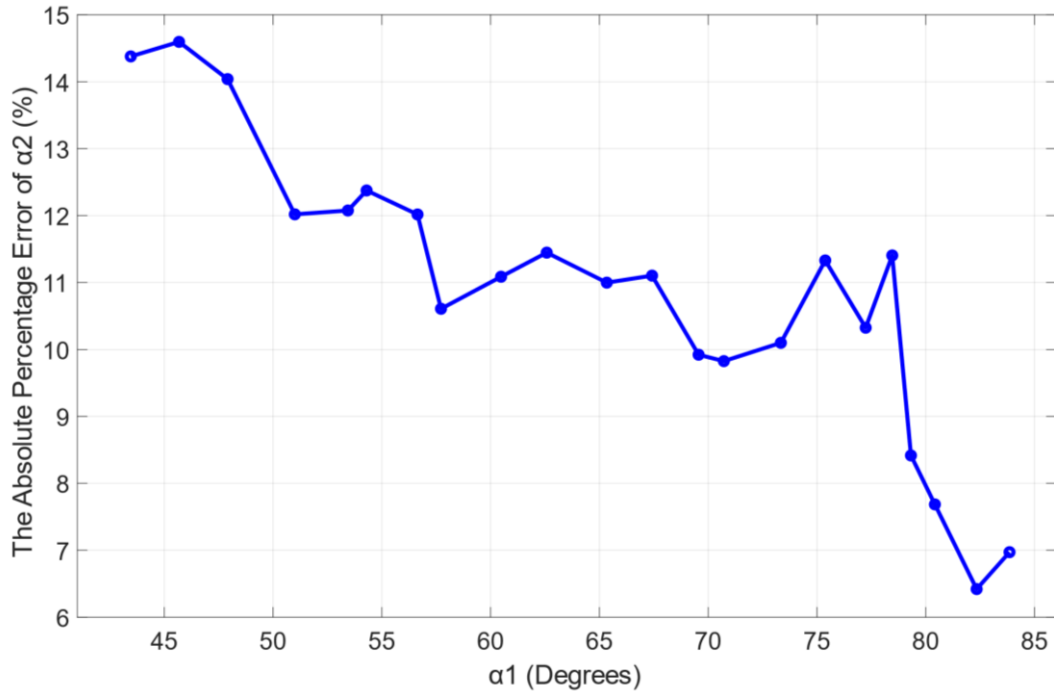
**Figure 4.25.** The calculated results from the numerical solution, the approximated line, the simulation, and the experiment with the 9 Ah battery.

Figure 4.26 shows the calculated absolute percentage error when using the 12 Ah battery, the error calculation was made where the experimental result range is considered between 39.8° to 84.2°. The maximum error was calculated as 16.65% when the turn on angle was 69.4° and the input voltage amplitude was 14.28 V. The minimum error was calculated as 5.45% when the turn on angle was 84.2°, and the input voltage amplitude was 13.65 V.



**Figure 4.26.** The absolute percentage error of  $\alpha_2$  values between the numerical and the experimental results as a function of  $\alpha_1$  when using the 12 Ah battery.

The calculated absolute percentage error when using the 9 Ah battery is given in figure 4.27, the error calculation was made where the experimental result ranged between  $43.46^\circ$  to  $83.85^\circ$ . The maximum error was calculated as 14.59% when the turn on angle was  $45.68^\circ$  and the input voltage amplitude was 19.5 V. The minimum error was calculated as 6.37% when the turn on angle was  $82.34^\circ$  and the input voltage amplitude was 13.7 V.



**Figure 4.27.** The absolute percentage error of  $\alpha_2$  values between the numerical and the experimental results as a function of  $\alpha_1$  when the 9 Ah battery was used.

#### 4.5. Calculating the Time Constant of the Circuit

The series resistance of the MBR560 Schottky diode ( $r_s$ ) has been estimated to be 42.15 m $\Omega$  based on its characteristics. The equivalent time constant of the circuit with two conducting diodes can be determined using the provided equation 4.4. The time constant is approximately 20% of the electrical period. The primary factors contributing to deviations between simulations and experimental results, as well as between the analytical model and experimental results, are the series resistance exhibited by the MBR560 Schottky diodes and their nonlinearity.

$$\tau = \frac{L_s}{2R} = 0.33e - 3 / (2 * 42.15e - 3) = 3.914 \text{ ms} \quad (4.4)$$

## 5. CONCLUSION

A detailed analytical model derivation was successfully presented to describe the nature of the relation between the conduction angles of the input current of a single-phase full-wave bridge rectifier having an AC side smoothing inductor and a constant voltage load, working in discontinuous conduction mode. The necessary assumptions needed to be made for the simplified version of the solution. The formula which describes the relationship between  $\alpha_1$  and  $\alpha_2$  is a nonlinear equation. It was only possible to solve it using a numerical method. Utilizing MATLAB, the solution was found, and it was shown that the conduction angles have almost a linear relation, indicating that their relation can be represented by a simple equation of the line.

Simulations of the proposed rectifier circuit topology were given to show the operation mode of the rectifier with the desired characteristics, that being mainly the discontinuous conduction mode, and constant voltage load, which was achieved successfully. Simulations were also attempted to achieve CCM in accordance with the analytical model prediction regarding this operation mode, but unfortunately, it did not match the model prediction. The simulation was also used to examine the relation between the conduction angles when the rectifier works in DCM, and it showed also an almost linear relation between them, which follows the numerical results well. The maximum calculated error between the simulation result and the numerical solution result was 14.4%. The implementation of the proposed system was done. It was found that a variable transformer was a necessary part of the system, to supply the rectifier with various input voltage values, the input current will vary accordingly, and a meaningful range of conduction angles would be calculated. The lead acid battery was shown to be a proper choice as a constant voltage load. It was found that high-tolerance-rated electronic components were necessary to be used to handle high current values properly. The oscilloscope was proven to be a convenient measurement instrument with accurate reading results, which it provided, besides its ability to send the acquired data to MATLAB for further processing. The current probe provided accurate readings with a simple operation. Exchanging data between the oscilloscope and MATLAB was done by integrating SCPI language commands into the

programming environment of MATLAB. An algorithm consisting of several stages of communication between them was needed to plot the measurements' waveforms properly and calculate the conduction angles of the input current. It was shown that the conduction angles acquired from the practical rectifier system while working in DCM also have an almost linear relation. It was found that the maximum percentage error of the turn off angle ( $\alpha_2$ ) calculated between the numerical result and experimental result was 16.65% when the 12 Ah battery load was used, and it was 14.59% when the 9 Ah battery load was used.

## REFERENCES

- [1] Muhammad H. Rashid, *POWER ELECTRONICS HANDBOOK DEVICES, CIRCUITS, AND APPLICATIONS*, 3rd ed.
- [2] “Rectifier Applications Handbook Reference Manual and Design Guide,” 2001. [Online]. Available: <http://onsemi.com>
- [3] M. WCIŚLIK and P. STRZĄBAŁA, “Analytical model of single-phase AC circuit with inductance and bridge rectifier.,” *Przegląd Elektrotechniczny*, vol. 94, no. 3, pp. 126–129, 2018, doi: 10.15199/48.2018.03.24.
- [4] P. Strzabala and M. Wcislik, “Impact of the Ripple Output Voltage of the Bridge Rectifier on the Equivalent Parameters of the AC Circuit in Continuous Mode,” in *2018 Progress in Applied Electrical Engineering (PAEE)*, IEEE, Jun. 2018, pp. 1–7. doi: 10.1109/PAEE.2018.8441138.
- [5] J. Gnanavadivel, P. Yogalakshmi, N. Senthil Kumar, and K. S. Krishna Veni, “Design and development of single phase AC–DC discontinuous conduction mode modified bridgeless positive output Luo converter for power quality improvement,” *IET Power Electronics*, vol. 12, no. 11, pp. 2722–2730, Sep. 2019, doi: 10.1049/iet-pe.2018.6059.
- [6] B.-R. Lin and T.-S. Hwang, “Single phase rectifier with high power factor in continuous and discontinuous conduction mode,” in *Proceedings of the IEEE International Symposium on Industrial Electronics*, Athens, Greece: IEEE, 1995, pp. 421–426. doi: 10.1109/ISIE.1995.497034.
- [7] A. Tokic, A. Jukan, and J. Smajic, “Parameter Estimation of Single-Phase Rectifier-Based Loads: Analytical Approach,” *IEEE Transactions on Power Delivery*, vol. 31, no. 2, pp. 532–540, Apr. 2016, doi: 10.1109/TPWRD.2015.2424914.
- [8] D. Yan and A. Kwasinski, “Study of a single-phase full-wave uncontrolled rectifier with a constant power load,” in *2018 IEEE International Telecommunications Energy Conference (INTELEC)*, IEEE, Oct. 2018, pp. 1–7. doi: 10.1109/INTLEC.2018.8612342.
- [9] J. Drapela, R. Langella, A. Testa, and V. Vendemia, “A New Analytical Model of Single-Phase Diode Bridge Rectifiers in the Presence of Interharmonics in Supply Voltage,” *IEEE Open Access Journal of Power and Energy*, vol. 10, pp. 385–394, 2023, doi: 10.1109/OAJPE.2023.3244330.
- [10] Y. Yin *et al.*, “Detailed Theoretical Analysis and Simulation Verification of Diode Rectifier,” in *2023 6th International Conference on Energy, Electrical and Power Engineering (CEEPE)*, IEEE, May 2023, pp. 399–405. doi: 10.1109/CEEPE58418.2023.10166029.

- [11] N. N. Esfetanaj, S. Peyghami, H. Wang, and P. Davari, "Analytical Modeling of 9-150 kHz EMI in Single-Phase PFC Converter," in *IECON 2019 - 45th Annual Conference of the IEEE Industrial Electronics Society*, IEEE, Oct. 2019, pp. 4689–4693. doi: 10.1109/IECON.2019.8927705.
- [12] T. M. Mertens and R. M. Stephan, "Operation Boundaries of a Single Phase Thyristor Driven DC-Motor," in *2019 IEEE 15th Brazilian Power Electronics Conference and 5th IEEE Southern Power Electronics Conference (COBEP/SPEC)*, IEEE, Dec. 2019, pp. 1–6. doi: 10.1109/COBEP/SPEC44138.2019.9065761.
- [13] M. Weislik, "The analytical model of steady-state of three-phase circuit with nonlinear load," in *2017 Progress in Applied Electrical Engineering (PAEE)*, IEEE, Jun. 2017, pp. 1–6. doi: 10.1109/PAEE.2017.8008986.
- [14] A. Di Gerlando, G. M. Foglia, M. F. Iacchetti, and R. Perini, "Comprehensive steady- state analytical model of a three- phase diode rectifier connected to a constant DC voltage source," *IET Power Electronics*, vol. 6, no. 9, pp. 1927–1938, Nov. 2013, doi: 10.1049/iet-pel.2013.0026.
- [15] P. Pejovi and J. W. Kolar, "An Analysis of Three-Phase Rectifiers with Constant Voltage Loads," in *5th European Conference on Circuits and Systems for Communications (ECCSC)*, IEEE, 2010, pp. 119–126.
- [16] J. A. M. Bleijs, "Continuous conduction mode operation of three-phase diode bridge rectifier with constant load voltage," *IEE Proceedings - Electric Power Applications*, vol. 152, no. 2, p. 359, 2005, doi: 10.1049/ip-epa:20040684.
- [17] Y. V. Singh, P. O. Rasmussen, and T. O. Andersen, "Performance improvement of three phase rectifier by employing electronic smoothing inductor," in *IECON 2014 - 40th Annual Conference of the IEEE Industrial Electronics Society*, IEEE, Oct. 2014, pp. 1713–1719. doi: 10.1109/IECON.2014.7048733.
- [18] Y. V. Singh, P. O. Rasmussen, T. O. Andersen, and H. Shaker, "Modeling and control of three phase rectifier with electronic smoothing inductor," in *IECON 2011 - 37th Annual Conference of the IEEE Industrial Electronics Society*, IEEE, Nov. 2011, pp. 1450–1455. doi: 10.1109/IECON.2011.6119521.
- [19] K. Jaitrong, S. Phonsri, and M. Kupimai, "A modify technique to actively damp oscillation in the input LC filter of Three-phase PWM rectifier," in *2008 5th International Conference on Electrical Engineering/Electronics, Computer, Telecommunications and Information Technology*, IEEE, May 2008, pp. 1017–1020. doi: 10.1109/ECTICON.2008.4600605.
- [20] J. Mauro, T. Roettger, and M. Superczynski, "Average model of a three phase controlled rectifier valid for continuous and discontinuous conduction modes," in *2015 IEEE Transportation Electrification Conference and Expo (ITEC)*, IEEE, Jun. 2015, pp. 1–7. doi: 10.1109/ITEC.2015.7165798.
- [21] R. M. Cuzner and G. Venkataramanan, "Current Source Rectifiers in Discontinuous Conduction Modes of Operation," *IEEE Trans Ind Appl*, vol. 51, no. 1, pp. 470–478, Jan. 2015, doi: 10.1109/TIA.2014.2334732.



- [22] F. Degioanni, I. G. Zurbriggen, and M. Ordonez, "Improved Control for Three-Phase Rectifiers with Constant Power Loads," in *2023 IEEE Applied Power Electronics Conference and Exposition (APEC)*, IEEE, Mar. 2023, pp. 2775–2779. doi: 10.1109/APEC43580.2023.10131411.
- [23] Z. Zhao, Q. Gao, K. He, and J. Tang, "Boundary and optimum of constant-voltage load three-phase bridge rectifier," in *2014 17th International Conference on Electrical Machines and Systems (ICEMS)*, IEEE, Oct. 2014, pp. 3192–3198. doi: 10.1109/ICEMS.2014.7014042.
- [24] K. Areerak, T. Sopapirm, S. Bozhko, C. I. Hill, A. Suyapan, and K. Areerak, "Adaptive Stabilization of Uncontrolled Rectifier Based AC–DC Power Systems Feeding Constant Power Loads," *IEEE Trans Power Electron*, vol. 33, no. 10, pp. 8927–8935, Oct. 2018, doi: 10.1109/TPEL.2017.2779541.
- [25] Q. Du, F. Meng, and L. Gao, "Analytical Model of Series-Connected 12-Pulse Rectifier with Constant-Voltage Load," in *2019 22nd International Conference on Electrical Machines and Systems (ICEMS)*, IEEE, Aug. 2019, pp. 1–6. doi: 10.1109/ICEMS.2019.8921789.
- [26] L. Chen and Y. Xie, "Analysis of Three-Phase Bridge Rectifier with Constant Voltage Loads," in *2010 International Conference on Electrical and Control Engineering*, IEEE, Jun. 2010, pp. 3347–3350. doi: 10.1109/iCECE.2010.816.
- [27] K. Basu, A. K. Sahoo, V. Chandrasekaran, and N. Mohan, "Grid-Side AC Line Filter Design of a Current Source Rectifier With Analytical Estimation of Input Current Ripple," *IEEE Trans Power Electron*, vol. 29, no. 12, pp. 6394–6405, Dec. 2014, doi: 10.1109/TPEL.2014.2305435.
- [28] S. Rajasekar, V. Karthikeyan, and N. Kumaresan, "Experimental Validation of CCM and DCM Operations of Semi-Bridgeless Boost Rectifier for Power Quality Improvement in UPS System," in *2018 20th National Power Systems Conference (NPSC)*, IEEE, Dec. 2018, pp. 1–6. doi: 10.1109/NPSC.2018.8771813.
- [29] John G. Kassakian, Marting F. Schlecht, and George C. Verghese, *Principles of Power Electronics*. Addison Wesley Publishing Company, 1991.
- [30] R. Boylestad, L. Nashelsky, and P. Hall, *ELECTRONIC DEVICES AND CIRCUIT THEORY*, 7th ed.
- [31] Adel S. Sedra, Kenneth C. Smith, Tony Chan Carusone, and Vincent Gaudet, *Microelectronic Circuits (The Oxford Series in Electrical and Computer Engineering)*, 8th ed. Oxford University Press, 2019.
- [32] P. Horowitz and W. Hill, *THE ART OF ELECTRONICS*, 3rd ed. 2015.
- [33] R. Priemer, *MATLAB for Electrical and Computer Engineering Students and Professionals with Simulink*. SciTech Publishing, 2013.
- [34] James V. Stone, *Linear Regression With Matlab: A Tutorial Introduction to the Mathematics of Regression Analysis*. Sebtel Press, 2022.
- [35] Inc. Cadence Design Systems, "Orcad ® Capture User's Guide," 2000. [Online]. Available: [www.orcad.com/technical/technical.asp](http://www.orcad.com/technical/technical.asp)

- [36] Inc. Cadence Design Systems, “PSpice® PSpice A/D, PSpice A/D Basics, and PSpice User’s Guide,” 2000. [Online]. Available: [www.orcad.com/technical/technical.asp](http://www.orcad.com/technical/technical.asp)
- [37] C. K. Alexander and M. N. O. Sadiku, *Fundamentals of electric circuits*, 6th ed.
- [38] “Understanding the Operation and Applications of Variable Transformers - Technical Articles.” Accessed: Oct. 28, 2023. [Online]. Available: <https://eepower.com/technical-articles/variable-transformers-operation-and-applications/#>
- [39] “Compact Technology Corp. MBR560 Schottky Barrier Rectifiers Datasheet.” Accessed: Jan. 16, 2024. [Online]. Available: <https://html.alldatasheet.net/html-pdf/333174/CTC/MBR560/53/1/MBR560.html>
- [40] IOTech In, *Instrument Communication Handbook : A handbook of IEEE 488, RS-232, SCPI, SCSI and Other Interfacing Standards*, First Edition. 1991.
- [41] “Programming Guide MSO1000Z/DS1000Z Series Digital Oscilloscope,” 2015. [Online]. Available: [www.rigol.com](http://www.rigol.com)
- [42] Roland Szabó, Aurel Gontean, Ioan Lie, and Mircea BăbăiŃă, “Oscilloscope Control with PC,” *INTERNATIONAL JOURNAL OF COMPUTERS AND COMMUNICATIONS*, vol. 3, no. 3, 2009, Accessed: Sep. 17, 2023. [Online]. Available: <http://www.universitypress.org.uk/journals/cc/19-396.pdf>
- [43] Walt. Kester and Analog Devices Inc., *Analog-Digital Conversion*. Analog Devices, 2004.
- [44] M. Crescentini, S. F. Syeda, and G. P. Gibiino, “Hall-Effect Current Sensors: Principles of Operation and Implementation Techniques,” *IEEE Sens J*, vol. 22, no. 11, pp. 10137–10151, Jun. 2022, doi: 10.1109/JSEN.2021.3119766.
- [45] Honeywell, *MICRO SWITCH Sensing and Control HALL EFFECT SENSING AND APPLICATION*.
- [46] “CC-65 AC/DC CURRENT CLAMP OPERATOR’S MANUAL.”
- [47] P. Ekdunge, “A simplified model of the lead/acid battery,” *J Power Sources*, vol. 46, no. 2–3, pp. 251–262, Oct. 1993, doi: 10.1016/0378-7753(93)90023-T.

## **CURRICULUM VITAE**

Name Surname: Abdullah Waleed Jalil AL-SALIHI

### **EDUCATION:**

**Undergraduate** : 2019, Iraq, University of Diyala, College of Engineering,  
Department of Electronic Engineering.

**Graduate** : 2024, Sakarya University, Institute of Natural Sciences,  
Department of Electrical and Electronics Engineering.

### **PUBLICATIONS, PRESENTATIONS AND PATENTS ON THE THESIS:**

Abdullah W. AL-SALIHI, Şuayb Çağrı YENER (2023, September). An Automated System for the Electrical Measurements of a Rectifier Circuit Using SCPI. 3rd International Conference on Innovative Academic Studies ICIAS 2023 on September 26-28, 2023 in Konya, Turkey.

### **LANGUAGES:**

Arabic, English.